Chemical heterogeneity of Mt. Etna magmas in the last 15 ka. Inferences on their mantle sources

Rosa Anna Corsaro[1], Nicole Métrich[2,3]

[1] Istituto Nazionale di Geofisica e Vulcanologia, sezione di Catania - Osservatorio Etneo, Catania, Italy

[2] Institut de Physique du Globe, CNRS UMR-7154, Sorbonne Paris-Cité, Univ. Paris Diderot, F-75005 Paris, France

[3] Istituto Nazionale di Geofisica e Vulcanologia, sezione di Pisa, Italy

Corresponding author*

Rosa Anna Corsaro

Istituto Nazionale di Geofisica e Vulcanologia

Sezione di Catania - Osservatorio Etneo

Piazza Roma 2, 95125 Catania, Italy

Keywords: Mt Etna, geochemistry, mantle source, basalts, alkali-enrichment

Highlights

We focus on the primitive basaltic magmas that bypassed Etna central conduits

Magma heterogeneities are linked to the melting of heterogeneous Hyblean-type mantle

None of the pre-1970s magmas are parent of present-day basalts

The ongoing selective alkali-enrichment of Etna magmas is a mantle source process

The decoupling of Rb-K and ^{87}Sr-Cl reveals multistage events of mantle metasomatism

Abstract
Primitive basaltic magmas are crucial in the study of the geochemical heterogeneity documented in Etna magmas and their inferred mantle sources. We undertook a systematic sampling of the less evolved basalts (Mg# >50) erupted over last 15 ka, a time period which corresponds to the activity of the youngest volcanic edifice of Mt. Etna complex, i.e. Mongibello volcano. We focused on lava flows and pyroclastites emplaced during '*deep-dyke fed'* (DDF) eruptions which were driven by the rapid ascent of deeply-rooted magma intrusions that bypassed the shallow plumbing system of the volcano. All the samples were analyzed by the same laboratory to avoid analytical bias, to build a comprehensive dataset on their major and trace element compositions and to propose a coherent framework for interpreting the geochemical fingerprints of present-day Etna basalts.

Trace element modelling, together with literature data for Sr isotopes, gave insight into long-term magmatic processes related to different melting degrees of the heterogeneous mantle beneath Mt Etna. *DDF* magma batches provide good snapshots of their mantle source heterogeneities that point to the variable involvement of clinopyroxenitic lithology, Rb-^{87}Sr-Cl-rich fluid component(s) possibly controlled by their source mineralogy, and slab-derived fluids selectively enriched in alkalis (Rb, K). The ongoing alkali (Rb, K) enrichment of the present-day magmas, well manifest since the 1970s, is decoupled from that of Sr and Cl. We propose that this process is linked to mantle source composition and is concomitant with changes in both volcanological and seismotectonic patterns of the volcano. There is no time evolution of *DDF* magma chemistry.

Keywords: Mt. Etna, geochemistry, mantle source, basalts, alkali-enrichment

1. Introduction

Etna is located in a complex tectonic setting at the African-European-Ionian plate junction (Goes et al., 2004) where: (i) the Apennine–Maghrebian Chain overlaps the undeformed African continental plate margin (e.g., Bousquet and Lanzafame, 2004), (ii) a diffuse transform boundary has formed across northeastern Sicily to connect the Sicilian and Calabrian plate boundaries (Goes et al., 2004), and (iii) the asthenospheric mantle flow upraises passively from under the neighbouring African plate, possibly in relation to the backwards migration and rollback of the Ionian slab (Gvirtzman and Nur, 1999). The related mantle heterogeneity beneath Mt. Etna and its imprint on the magma geochemistry have been intensely debated (e.g. Armienti et al., 2004; Viccaro and Cristofolini 2008). On a broader scale, the nature of the lithosphere beneath southeastern Sicily has been the subject of a recent controversy (e.g. Manuella et al., 2013, 2014; Beccaluva et al., 2013). The source region of Etna present-day magmas has been hypothesized to involve a HIMU-type component (high Pb isotope ratios and relatively low $^{87}Sr/^{86}Sr$ ratio), together with an enriched component (EM1) related to the recycling of subducted continental crust, or marine sediments, or altered oceanic crustal material (see Corsaro and Pompilio, 2004; Viccaro et al., 2008 for reviews).

Many studies have focused on the alkali (K, Rb, Cs) and Sr enrichment of Etna magmas erupted since the 1970s (e.g. Condomines et al., 1995) that was attributed to interaction between an OIB-type mantle source and a slab-derived component (Schiano et al., 2001), or slab-derived fluids enriched in B, $\delta^{11}B$ and fluid-mobile elements (Tonarini et al., 2001; Armienti et al., 2004). Shallow magma contamination by the flyshoid sedimentary lithologies that constitute the upper part of Mt. Etna basement (Clocchiatti et al., 1988) was acknowledged by Tonarini et al., (2001), but also ruled out as the main process because the alkali enrichment of Etna magmas is recorded by olivine-hosted melt inclusions entrapped at high pressure (> 400 MPa) and deeper than the sedimentary basement (Métrich et al., 2004; Spilliaert et al., 2006). An alternative process of magma contamination by supercritical fluids carrying chlorine and alkalis has also been recently advocated (Ferlito and Lanzafame, 2010; Ferlito et al., 2014) a hypothesis that we will discuss below in light of melt inclusion data. On the other hand, Etna primitive magmas were considered to derive from melting of a Hyblean-type peridotite lithology veined with a clinopyroxenite lithology (Correale et al., 2014). This hypothesis is corroborated by (i) the similarity in Sr isotopes and trace element geochemistry between the Hyblean mafic magmas and Mt. Etna tholeiites (Trua et al., 1998; Correale et al., 2015), and (ii) the recognition of Ca-rich magmas as bulk rocks (3930 BP eruption; Coltelli et al., 2005),

and melt inclusions (Kamenetsky et al., 2007). Variable extents of melting of a mantle source heterogeneously affected by metasomatic fluid influx have been proposed by several authors (Kamenetsky and Clocchiatti, 1996;Viccaro and Cristofolini, 2008). By contrast, temporal variations of the $^{3}He/^{4}He$ ratio reported for Etna mantle source are negligible (6.7±0.4 *R*a, Marty et al., 1994; 6.5-6.7 *R*a, Nuccio et al., 2008; 6.61±0.15 *R*a, Coulson et al., 2011) or very limited (7.6-6.6 *R*a, Correale et al., 2014).

The geochemical heterogeneity of Mt. Etna basalts and the nature of their sources are still opened questions and the parent magma of present-day basalts has not been satisfactorily constrained because: (i) Etna basalts with Mg# >0.50 and Ni content > 27 ppm are scarce; (ii) most studies are based on only a very few samples which are not thoroughly described and not even well located; (iii) discussions are commonly based on lavas derived from shallow parts of the plumbing system where magma mixing prevails (e.g. Métrich et al., 2004; Corsaro and Pompilio, 2004), which may prevent identification of the geochemical fingerprints of the parent magmas and of their sources, and (iv) in some cases, the geochemical data are provided from different laboratories using different techniques that may create analytical biases.

As an example, one lava sample (7.75 wt% MgO) from Mt. Maletto, a monogenetic Holocene cone on Mt. Etna, has been regarded as the most primitive basalts (Tanguy, 1980; Armienti et al., 1988; Condomines at al., 1995; Kamenetsky and Clocchiatti, 1996). It has been used as the parent magma to model the differentiation paths of Etna present-day basalts (Armienti et al., 2004). However, Mt. Maletto lava carries high-Mg olivine (Mg# 0.88-0.90) xenocrysts which are not in equilibrium with their host, and contain Ca-rich picritic melt inclusions (Kamenetsky and Clocchiatti 1996), very similar in composition to the 3930 BP picrites (Kamenetsky et al., 2007). These crystals cannot be directly linked with this later picrite because the eruptions site are located on different areas of the volcano (Fig. 1), but they could testify to the existence of picritic magma older than the 3930 BP eruption.

To get a better overview of chemical compositions of Mt. Etna primitive basalts we collected new representative samples of lavas and scoriae emplaced during the '*deep-dyke fed' (DDF)* eruptions, which were driven by the rapid ascent of deeply-rooted magma intrusions that bypassed the volcano central conduits (Corsaro et al., 2009b and references therein). These eruptions occurred in a time period (15 ka - present) which corresponds to the activity of the youngest edifice of Mt. Etna complex, i.e. Mongibello volcano. In sampling, we took into account the geological features (i.e. lava flow extension) reported in the new geological map of Mt. Etna (Branca et al., 2011). All the analyses were performed by the same laboratory to ensure the self-consistency of our dataset. The dataset is also fully comparable to published

geochemical data on Etna basalts extruded during other historic *DDF* eruptions – 1763 A.D. La Montagnola (Corsaro et al., 2009b), 1974 A.D. (Corsaro et al., 2009b), 2001 A.D. (Corsaro et al., 2007) and 2002-03 A.D. (Corsaro et al., 2009a) - which were carried out in the same facility, and are integrated in our database. As a whole, the trace element data provide evidence of variable degrees of melting of a heterogenous mantle source beneath Mt. Etna and of the absence of time-related alkali-enrichment of Etna basalts from 15 ka to the present.

2. Sampling, sample mineralogy and chemistry

2.1. Sampling

Our study covers a broad time span (15 ka-present) associated to the activity of the Mongibello volcano. As illustrated in Figure 1, the sample sites are few, but we focused solely on the monogenetic scoria cones and the pyroclastic sequences which produced primitive basalts on Mt. Etna in the time of interest: M.te Frumento delle Concazze, hereafter Mt. Frumento (3540±70 BP; Del Carlo et al., 2004); Mt. Maletto dated 7000 yr BP by Condomines et al., (1995); Mt. Spagnolo (15ka - 3930±60 BP; Branca et al., 2011), and the 3930±60 BP pyroclastic deposit (FS picritic tephra of Coltelli et al., 2005). We collected a total of 25 samples (17 from Mts. Maletto, Spagnolo and Frumento lava flows and 8 from three pyroclastic deposits, i.e. Mts. Frumento and Maletto cones and FS tephra). In each case, 5 to 7 lava samples were collected to cover as wide an area as possible to track space-dependent geochemical variability.

Figure 1

2.2. Petrography

Mt. Maletto (MAL) lavas and scoriae are sub-aphyric (phenocryst proportion < 5 vol.%) with idiomorphic clinopyroxene, up to 0.5 mm in size, which are more abundant than olivine crystals, smaller than 0.5 mm. High Mg-olivine (Fo ~88-90) and Cr-rich diopside found in MAL lava samples are not in equilibrium with their carrier host magmas (Kamenetsky and Clocchiatti, 1996; Métrich, unpublished data). Mt. Spagnolo (MSP) and Mt. Frumento (MFR 5, 6 and 7) lavas are slightly more porphyritic (5-10 vol.% phenocrysts), with similar proportions of idiomorphic clinopyroxene (0.5 to 1-1.5 mm) and olivine (up to 0.5-1 mm). The

lava groundmass texture varies from micro- to crypto-crystalline. Idiomorphic plagioclase phenocrysts are present only in a part of the MFR samples (MFR1, 2, 3 and 4; 10 vol.% of phenocrysts). It complements the paragenesis made prevalently of clinopyroxene (Fe-rich augite) and olivine Fo <82 (Métrich, unpublished data). The bimodal distribution of MFR lava chemical composition having distinct mineral paragenesis is consistent with the mingling/mixing between basaltic and hawaiitic magmas which have been identified in Mt. Frumento lava bombs (Clocchiatti and Métrich, 1986). Finally, the 3930 BP scoriae (FS) are crystal-poor (< 9 vol.%) but contain the most primitive paragenesis that consists of Mg-rich olivine (Fo ≥ 90), Cr-rich diopsidic pyroxene phenocrysts and subordinate spinel in agreement with the earlier studies of Kamenetsky et al. (2007).

2.3. Major and trace element compositions of bulk rocks

The major and trace element contents of bulk rocks (Table 1) were measured using Inductively Coupled Plasma Optical Emission Spectroscopy (ICP-OES) and Inductively Coupled Plasma–Mass Spectrometry (ICP-MS), respectively (Carignan et al., 2001), at the Centre de Recherches Pétrographiques et Géochimiques (SARM) in Nancy (France). Analytical uncertainty (1σ) is: <1% for SiO_2 and Al_2O_3, <2% for Fe_2O_3, MgO, CaO, Na_2O, K_2O, <5% for MnO, and TiO_2 and 5–10% for P_2O_5, and <5% for all trace elements except U (<8%). For the detail of analytical uncertainty see Table S1 (auxiliary material).

Table 1

Figura 2

Figure 3

Major elements (Fig. 2) fully confirm that the FS tephra (13.6±1.3 wt% of MgO on average) represents the least evolved magma identified during the recent eruptive history of Mt. Etna and that it differs from the others by its anomalously high CaO content (Fig. 3), as previously reported (Kamenetsky et al., 2007).

Plagioclase-free basalts (MAL, MSP, MFR) have similar MgO contents and CaO/Al_2O_3 ratios but they display distinct alkali contents and FeO_{total}/MgO ratios (Fig. 2c, d). By "plagioclase-free" we mean that plagioclase is not present as phenocrysts but may crystallize as microlites within the groundmass. The observed major element variations cannot be explained by a single process of fractional crystallization but also require source processes. The

most evolved samples are represented by the plagioclase-bearing lavas of Mt. Frumento (samples MFR1, 2, 3 and 4), which are homogeneous and for which MgO averages at 6.4±0.3 wt%. These share similar MgO contents with average Etna magmas (6.27±0.26 wt%; N = 33) erupted during the last few decades (*DDF* eruptions of 1974, 2001, 2002-03), but they differ in their lower CaO content and CaO/Al_2O_3 ratio (Fig. 2b, d). The chemical variations found in Mt. Frumento (plagioclase-bearing and plagioclase-free) samples are consistent with a differentiation trend prevalently governed by crystal fractionation (see section 3).

Figure 4

Trace element compositions span a large compositional range whose most primitive end-member (MgO from 14.6 to 12.2 wt%; Ni from 215 to 125 ppm) is the FS tephra (Fig. 4). The most important feature is the significant range of incompatible elements (Fig. 4 a-c) measured in plagioclase-free basalts for a restricted variation of their Co contents (from 46 to 34 ppm) and thus for basalts having a similar degree of differentiation (MAL, MSP, MFR). These observations exclude a dominant role for crystal fractionation. On the contrary, the high incompatible trace element (Ta, Rb, Ba, La) contents of the most evolved plagioclase-bearing lava flow of Mt. Frumento (samples MFR1-4) likely result from crystal fractionation as we will present in the next section. More broadly the overall evolution trend of these two elements Co and Ta (Fig. 4d) which are, respectively, highly compatible and highly incompatible requires a combination of crystal fractionation and magmatic source processes.

Figure 5

In Figure 5, the trace element concentrations normalized against global MORB values (Arevalo and McDonough, 2010) show common features for all Etna *DDF* basalts: (i) similar patterns despite variable levels of the element enrichment/depletion; (ii) systematic, but slight, negative anomalies in high field strength elements (Nb, Ta, Hf, Zr) that are widely accepted to reflect the imprint of slab-derived fluids in arc magmas (e.g. Tatsumi 1989), and (iii) relative enrichments in LILE (K, Ba and Rb) and LREE (La/Yb ratio from 14.5 to 38.0). Hence, several lines of reasoning suggest the involvement of slab-derived fluids in the *DDF* magma source at Mt. Etna, as proposed also to explain the radiogenic Sr and high $\delta^{11}B$ signature of recent Etna lavas (Tonarini et al., 2001), the melt inclusion geochemistry (Kamenetsky and Clocchiatti,

1996; Schiano et al., 2001), and their high volatile concentrations (H_2O, S, Cl; Métrich et al., 2004; Spilliaert et al., 2006; Corsaro et al., 2009b). Relative enrichment in Nb (high Nb/Zr ratio, from 0.14 to 0.29) with respect to global MORB (Nb/Zr = 0.06) is also fully consistent with an OIB-type mantle source further enriched by slab (Tonarini et al., 2001, Schiano et al., 2001). As such, the primitive basalts studied in this work represent fully the geochemical features typical of Etna magmas.

Finally, we would like to underline that the most and least enriched plagioclase-free basalts of the entire dataset are, respectively, Mt. Frumento (3540±70 BP; Del Carlo et al., 2004) and FS tephra (3930±60 BP; Coltelli et al., 2005) which, taking into account the eruption date, may be considered as contemporary.

2.4. Melt inclusion data: focus on chlorine

Ferlito et al. (2014) proposed a mechanism of Cl-rich fluids upward migration to explain the alkali (K, Rb) enrichment of the post-1970s magmas erupted at Mt. Etna. Shallow melt-vapor interaction, involving a Cl-S-H_2O-CO_2 bearing gas phase, has also been argued to account for the selective enrichment of semi-volatile element such as Cu in Etna magmas erupted in 2004-2007 (Collins et al., 2009). Chlorine has been extensively analyzed in olivine-hosted melt inclusions of basalts emplaced during the 1763, 1974, 2001 and 2002-03 *DDF* eruptions and has been proven a discriminating element between the pre- and post-1970s basalts (Corsaro et al., 2009b). In order to discuss the relationship between Cl and K we have integrated the dataset with new results for our samples of Mt. Frumento and the FS scoriae, as well as with a series of measurements on samples from strombolian activity which occurred between 1995 and 1999 at the summit craters: North-East crater (NEC 060696, NEC 271195) and Voragine (VOR 040999, VOR 060898) (Métrich and Corsaro, unpublished data). The data for Mt. Maletto are available in the literature (Schiano et al., 2001). Only the lava samples of Mt. Spagnolo were not considered because of the lack of suitable melt inclusions for volatile analyses.

Both melt inclusions and matrix glasses were analyzed using the SX50 CAMECA electron microprobe (CAMPARIS, Paris, France) with the procedure described in Spilliaert et al. (2006). Major elements were measured with a 10 nA beam current, 10 µm spot size, and a counting time of 10 to 25 sec, and Cl and P with a 30 nA beam current, a 15 µm spot size, and 200 sec. counting time on peaks. The data are reported in Table 2 and the accuracy of the analyses was checked against internal and international reference glasses (Table S2, auxiliary material).

Figure 6

Table 2

As a whole, the Cl concentrations analyzed in melt inclusions (MIs) hosted in olivine Fo ≥88 vary from 0.18 to 0.28 wt% in *DDF* basalts (FS, MAL, MFR) that fully confirm the enrichment of Etna basalts in Cl (Fig. 6a) as can be observed in arc basalts (e.g. Ruscitto et al., 2012). The most important point is the range of Cl/K_2O ratio values from 0.21±0.03 down to 0.08±0.01, that characterized the 2001-2003 *DDF* magmas. The data scatter is much more pronounced for MIs in olivine Fo_{80}-Fo_{70} analyzed from scoriae ejected during explosive summit activity in 1995-1999 (Fig. 6b). Most plot along and extend the 2001-2003 trend. The highest concentrations in both Cl and K_2O are consistent with crystal fractionation. The lowest Cl concentrations are akin to those of matrix glasses and point to the effect of degassing. The most striking feature is the presence of MIs, which are trapped in FeO-rich olivine (Fo_{76-70}) and record Cl concentrations and Cl/K_2O values as high as those measured in the pre-1970s magmas. Chlorine-rich inclusions are found in pyroclastites of the North-East Crater in 1995-1996 and Voragine in 1998-1999. Similar features were described in the 2005-2007 samples reported by Collins et al. (2009).

3. Fractional crystallization

To simulate the evolutionary trend of Mt. Frumento lavas, we performed mass balance calculations on the basis of major elements, starting from the most primitive basalt (average composition of the samples MFR 5, 6 and 7). Mineral phase compositions are taken from literature data for plagioclase (An_{83}, Corsaro et al., 2007), olivine (Fo_{87} and clinopyroxene (Mg#=89; Kamenetsky and Clocchiatti, 1996). Removal of 14 (wt)% solid consisting of 2% plagioclase, 4% olivine, 8% clinopyroxene, provides a good fit of the natural compositions of plagioclase-bearing MFR lavas (Fig.2; FC trend), with a relative error of less than 2%.

In addition we performed trace element modelling by using Rayleigh's equation and partition coefficients ($D^{mineral/melt}$) relevant for Etna magmas (D'Orazio et al., 1998). The good match between computed and natural compositions (within the analytical error <10%) is illustrated in Figure 4 (FC trend) and it fully confirms a dominant process of fractional crystallization to explain the compositional spectrum of MFR lavas. Hence, the MFR plagioclase-bearing basalts will not be considered in the further discussion about the possible nature of the mantle source(s) of Mt. Etna basalts.

4. Discussion

4.1. Trace element modelling: basic considerations

Mantle-derived xenoliths can provide information on the mantle source composition of a particular volcano but they are lacking at Mt. Etna where only rare crustal co-magmatic xenoliths have been identified (Lo Giudice and Rittmann 1975; Aurisicchio and Scribano 1987; Andronico et al. 2005; Corsaro et al., 2007; Corsaro et al., 2014 and references therein). Conversely, ultramafic mantle xenoliths in diatremes of Miocene age in the Hyblean region south of Etna, revealed the presence of pyroxenite-veined lithospheric mantle in their source (Sapienza and Scribano, 2000; Correale et al., 2014, 2015). The spatial proximity and the temporal continuity between the Hyblean and Etnean volcanic activities led Correale et al. (2014; 2015) to model the partial melting of a two-component mantle source to reproduce the composition of Mt. Etna primitive magmas to which the clinopyroxenite end-member is found to contribute some 10%. Their simulations start with a source composed of a mixture of HIMU-type peridotite (Zr/Nb~4, $^{143}Nd/^{144}Nd$~0.5129, $^{3}He/^{4}He$ ~7 *R*a) and pyroxenite (Zr/Nb~20 and $^{143}Nd/^{144}Nd$ ~0.5130; $^{3}He/^{4}He$~7.6 *R*a) with DMM-type geochemical affinity, in 90:10 relative proportions.

Our dataset allows us to refine the modelling of mantle source melting at Mt. Etna. Figure 7a presents the results of our calculations for non-modal fractional melting and accumulated fractional melting, as a function of the possible mineralogy of the mantle source and the degree of melting. Three Hyblean-type mantle sources have been considered in our models:

i) an *Hyblean mantle 1- type* consisting of an anhydrous spinel lherzolite comprising olivine (50-75%), orthopyroxene (8-25%), clinopyroxene (1-8%) and 1-3% spinel, with evidence of slight serpentinization as represented by the sample XIH-3 of Correale et al. (2012);
ii) an *Hyblean mantle 2- type* consisting of spinel peridotites with olivine, orthopyroxene, Cr-Al spinel, clinopyroxene and rare phlogopite. As a representative chemical composition we use the average of the samples UL-a23, UL-a8 and UL-a77 analyses that were published by Sapienza and Scribano (2000);
iii) an *Hyblean mantle 3-type* (Correale et al., 2014) formed by a mix of 90% *Hyblean mantle 1-type* and 10% pyroxenite (clinopyroxene ≥75% and orthopyroxene ≤5%). For our calculations we input the average chemical composition of samples XIP-4 and XIP-14 of Correale et al. (2012).

Initially, we considered a non-modal fractional melting scenario (Shaw, 1970) which implies that melting starts at the eutectic composition and that each increment of melt is instantaneously removed from the system after it is formed. The bulk partition coefficients and the proportions of melting (Ol:Opx:Cpx:Sp = 0.1:0.2:0.68:0.02) are from Strake et al. (2003; auxiliary material). The curves simulating the degrees of non-modal fractional melting of the three Hyblean-type mantle sources are plotted as dashed lines (labelled *Fractional melting*) in Figure 7a. For comparison, we have also modelled the fractional melting curves (grey dotted lines) of garnet-facies and spinel-facies depleted mantles, whose trace elements composition are from Salters and Stracke (2004). The bulk partition coefficients and proportions of melting are from Strake et al., (2003, auxiliary material).

Since fractional melting of Hyblean-like mantle sources does not fit at all Etna data, we have considered an alternative hypothesis. We modelled the 'accumulated fractional melting' (AFM) of the same sources according to which all the fractional melts accumulate and mix before eruption (Figure 7a, continuous lines labelled *Accumulated fractional melting*).

Figure 7

4.2 Geochemical tracking of Mt. Etna magma heterogeneity: inference on their mantle sources

In Figure 7a most Etna basalts plot between the fractional melting curves of garnet- and spinel-bearing depleted mantle. This feature is consistent with the derivation of Etna magmas from the mantle region extended across garnet-spinel transitions, in agreement with Viccaro and Cristofolini (2008). The presence of garnet in Etna mantle source is corroborated by trace element patterns of Etna basalts and the fractionation of heavy REE with respect to global MORB (Fig. 5). However, fractional melting implies very low degrees of melting (< 0.3%) for the Mongibello *DDF* magmas, regardless of the source composition.

Accumulated fractional melting of Hyblean-like peridotites could better reproduce the compositional trends of Etnean *DDF* magmas with degrees of melting varying from 15 to 8%, except for MFR basalts (<5%). We are aware that our modelling is not fully satisfactory because we are assuming that Hyblean xenoliths are representative of the mantle composition beneath Mt Etna in including clinopyroxenite-veins, water-bearing component(s) and a possible trace of serpentine. Moreover, melting may have occurred over a range of pressures and distinct time scales, and the crust thickness and the proportion of water available in the source may

drastically change the depth and the extent of melting, as well as the melt production (Asimow and Langmuir, 2006).

However, combining our trace element dataset with published (Correale et al., 2014; Corsaro et al., 2009a) and unpublished (Di Renzo) data on $^{87}Sr/^{86}Sr$ isotopes allows us to propose a general framework that may reconcile the main geochemical features of Mongibello basalts. Figure 8a illustrates the overall decrease of the Ta/Yb ratios from the MSP basalt to the 3930 BP (FS) picrite on which Rb-enrichment trends are superimposed. In such diagrams, variations of the Ta/Yb ratio track the depletion/enrichment of the mantle source, whereas increase in Rb/Th ratios typifies the slab-derived component(s). Figure 8b shows decoupling between Rb and ^{87}Sr enrichment in the post-1970s basalts. In each plot three end-members are recognized (MSP basalt, 2002-03 basalts and FS picrite).

Mt. Spagnolo basalt is confirmed to be one end-member that shares comparable Zr/Nb and Ce/Y ratios with Miocene Hyblean basalts and can be reproduced with ca. 8% melting of a spinel-peridotite (Hyblean mantle 2-type) mantle source (Zr/Nb = 3.5; Fig. 7b). It displays the highest Ta/Yb ratio (Fig. 8a) and the lowest values of the Rb/Th and $^{87}Sr/^{86}Sr$ ratios (Fig. 8b).

The 3930 BP (FS tephra) picrite, the other extreme end-member, requires greater degrees of melting (15%), but cannot fit with the accumulated fractional melting of a simple Hyblean peridotite (Zr/Nb = 6.6; Fig. 7b). It involves a significant contribution of a pyroxenite component (high Zr/Nb and low Ce/Y, Fig. 7a), as previously proposed (Kamenetsky et al., 2007) and calculated assuming flux melting of XIH-3 Hyblean peridotite by adding 0.01-0.3 wt% H_2O (Correale et al, 2014). The 3930 BP picrite is characterized by high Rb/Th (6.75) and $^{87}Sr/^{86}Sr$ (0.70391) ratios (Fig. 8a, b), but shares a similar Nd isotopic composition with MSP basalt ($^{143}Nd/^{144}Nd$ = 0.512836 and 0.512908, respectively, Correale et al., 2014; Table 1). The radiogenic signature of the FS sample is related to the high degree of melting and the largest contribution of clinopyroxenite lithology.

Basalts from Mt. Maletto, Mt. Frumento and 1763 *DDF* eruption plot between these two end-members (Fig. 8a, b). They display Rb-^{87}Sr enrichment observed for the 3930 BP FS tephra.

The post-1970s Etna basalts form another population (Fig. 8a, b). Interestingly, magmas emplaced during the *DDF* eruptions from 1763 to 2003 were generated by a comparable degree of melting from a slightly heterogeneous source (Fig. 7b) that is in agreement with similar values of their La/Sm ratios (6.50±0.2 for 1763; 6.08±0.06 for 1974; 6.1±0.2 for 2001-2009). However, the 1974 and 2001-2003 basalts clearly differ from the general trend of Rb-^{87}Sr enrichment (Fig. 8b) in being selectively enriched in Rb that points to the decoupling of these

two elements. Alkali-enrichment is thus independent of clinopyroxenite lithology in the mantle source. Figure 8a, in which literature data have been added to include products of flank and summit activity erupted from 1995 to 2009 (Andronico and Corsaro, 2011; Corsaro and Miraglia, 2014; Corsaro et al., 2009a; 2013), demonstrates the imprint of the alkali-enrichment of the post-1970s magmas. Hence, the 1970s were an important period when the still ongoing and increasing contribution of the alkali-bearing fluid component(s) on a heterogeneous mantle source tracked back.. Accordingly, none of the pre-1970s primitive magmas can produce the present-day basalts (Th ≤ 6 ppm; MgO ≤7.5 wt%) through crystal fractionation. Nor can the FS picrite (on average Th = 2.9 ppm, MgO = 13.5 wt%) be their parent magma because of its geochemistry (Fig. 8). This feature also excludes the hypothesis of the removal of a high amount of Mg-Ca rich solid that would be required to explain the difference in major and trace elements between the FS and Etna present-day magmas. Segregated minerals could have accumulated to build up the deeper part of the high Vp velocity body (HVB) as imaged, through seismic tomography, to extend down to the base of the crust (~18-20 km; Aloisi et al., 2002; Patanè et al., 2006). However, it has been shown that the HVB is made of intrusive gabbroic rocks which are not cumulative but are formed by *in-situ* crystallization at the solidification front of Etna's deep (>5 km b.s.l.) plumbing system (Corsaro et al. 2014).

In conclusion, *DDF* basaltic magma batches that are erupted through dykes that bypassed the volcano central conduits, sampled the chemical heterogeneity of their mantle sources. The Rb-^{87}Sr enrichment of the pre-1970s magmas is associated with Rb, ^{87}Sr, Cl-rich fluid component(s) in the mantle source, possibly inherited from an old recycling of crustal material, as proposed for the Hyblean region (Correale et al., 2014, 2015) and controlled by the mantle mineralogy. The selective enrichment of the post-1970s magmas is discussed in the light of our new Cl data in the next section. It is believed to be associated with distinct slab-derived fluids that overprinted a previously metasomatised mantle source (Fig. 7b; 8).

4.3. Alkalis in Etna magmas and chlorine-potassium decoupling

The selective enrichment in alkalis (K, Rb) of the post-1970s basalts is associated with a change in B isotopic compositions as reported for the 1992-1999 lavas (on average δ^{11}B = -3.75±0.4‰) with respect to pre-1970s lavas (δ^{11}B = -4.8±0.3‰; Tonarini et al., 2001). However, these lavas derived from the shallow reservoirs and are not representative of *DDF* magmas for which the δ^{11}B data are lacking. Extraction of alkalis from the basaltic magmas

ponding in the deep portion of Etna plumbing system (i.e. ~20 km) by a Cl-bearing H_2O, CO_2-rich phase, and their further transfer that could have caused the observed enrichment in the present-day magmas, has recently been advocated (Ferlito et al., 2014; Ferlito and Lanzafame, 2010). This process cannot be excluded but, as a general process, it is difficult to reconcile with the behaviours of Cl and Na_2O measured in Etna olivine-hosted melt inclusions (Figure 9). To avoid any bias related to crystal fractionation and to minimize the effects of the source melting degree, these two elements have been normalized to K_2O. Figure 9 shows that the FS, MAL and 1763 samples differ from the others in having the highest Cl/K_2O ratio (0.21±0.03). The Cl/K_2O ratio (0.08±0.01) of the post-1970s magmas is significantly lower than that measured in FS and MAL melt inclusions, for a limited range of Na_2O/K_2O ratio values (1.6-1.9), but is akin to values of Hyblean MIs (Schiano et al., 2001). Magmas (MIs) of the 1995-1999 summit activity dominantly plot within the 2001-2003 domain, whereas some of them tend towards the 1763 Cl-rich end-member. Systematic heterogeneity of MIs in 1995-2007 scoriae is fully consistent with interactions and connections between distinct magma pockets within Etna's shallow plumbing system (Kahl et al., 2011). It implies that magma batches having the pre-1970s geochemical characteristics are still present as residual bodies. This latter hypothesis is corroborated by the variability in trace elements (i.e. Rb/Nb ratio) and Sr-Nd isotopes of the magmas emitted from the summit craters in the period 1995-2001 (Corsaro et al., 2013) and is also confirmed by the contemporaneous emission of low and high-K trachybasalts from the eruptive fissures that opened in the North flank of the volcano during the 2002-03 eruption (Ferlito et al., 2009). There is no evidence of magma K-enrichment through alkali-bearing gas transfer, even though this process cannot be totally ruled out at the local scale.

Another important point to consider is the decoupling in the behaviours of Rb and ^{87}Sr. Indeed, the post-1970s *DDF* basalts depart from the general trend of Rb-^{87}Sr enrichment in having the highest Rb/Th ratio (up to 7) but they share a comparable Sr isotopic signature with Mt. Maletto basalt (Rb/Th = 4; Fig. 8b) erupted 7000 years ago. We suggest that these magmas tapped a heterogeneous,^{87}Sr-Cl-rich, clinopyroxenite-veined mantle beneath Mt. Etna that may have undergone several metasomatism events. We speculate that slab-derived fluids enriched in Rb could be related to the Etna geodynamic context, asthenospheric mantle diapir and the Ionian slab backwards migration and rollback (Gvirtzman and Nur, 1999). Whether these fluid components could be pore fluids or serpentine-derived fluids, or related to the breakdown of a K-Rb bearing mineral phase (i.e. phengite) in the slab itself are challenging questions that need further data on B-Sr-Nb-Pb isotopes on well characterized samples.

5. Concluding remarks

- Primitive basaltic magmas emplaced during *DDF* eruptions that built up several pyroclastic cones on Mt. Etna flanks during the activity of Mongibello volcano (15 ka-present) have varied in composition through time.
- Geochemical variations are not related with time; closely-spaced eruptions may produce basalts having the same degree of evolution but being variably enriched in incompatible elements.
- The behaviours of alkalis (K, Rb) and Cl (Sr-isotopes) in the post-1970s magmas are decoupled. Present-day Etna magmas are tapping a heterogeneous mantle source which experienced several stages of metasomatism. The contribution the slab-derived fluid possibly over-printed previous stages of metasomatism, even though a transfer of the alkalis by a Cl-bearing gas phase cannot be totally excluded at a local scale.
- Alkali enrichment of the post-1970s basalts is a unique process that represents a compositional watershed of Mongibello magmas.
- This chemical change was accompanied by modifications of both volcanological and seismotectonic patterns of the volcano in the early 1970s. Indeed, the eruption frequency, the cumulative volume of material from the flank eruptions, and the magnitude of volcanic events (i.e. occurrence of Subplinian eruptions) have significantly increased since this time (Branca and Del Carlo, 2004). A resumption of the seismic activity has been recorded (Azzaro et al., 2000), with strong earthquakes along main fault systems on the South (Timpe normal fault system) and Southwest (Ragalna transtensive structure) flanks of Mt. Etna (CMTE Working Group, 2014). Finally, since the 1970s the mean magma output rate (0.8 m^3/s) increased by a factor 4 with respect to the preceding 1759-1959 period (0.2 m^3/s; Harris et al., 2011). In agreement with these latter authors, high discharge rates are attributed to deep changes in the Etna plumbing system. Hence, the magma supply rate has increased too, since the volume of un-erupted magma is, on average, 3.3 times higher than of volume of extruded magma (Allard et al., 2006). These features strongly support the interplay between source processes, magma transport, the dynamics of the East flank sliding (e.g. Azzaro et al., 2013; Acocella et al., 2013 and references therein) but also extensional structures along the main rift zones of the volcano in connection with the regional tectonic regime (Monaco et al., 2005).
- Finally, we demonstrate that none of the *DDF* magmas erupted from 15 ka to 21st century can be considered as the parent magma of the basalts extruded during 2001 and 2002-03 eruptions. The geochemical variability of *DDF* magmas is better explained by varying extents of

accumulated fractional melting of Hyblean peridotite-type sources. These sources underwent several stages of metasomatism, most likely over a long timespan.

Acknowledgments

This work was funded by MED-SUV project. It is based on sampling which has been carried out with D. Andronico and L. Miraglia prior to the onset of this project. We thank them for the participation in the field work. We are also indebted to V. Di Renzo for making the Sr isotopic data of 2001 and Mt. Frumento delle Concazze eruptions available, not yet published. R. Azzaro and G. Puglisi are thanked for the helpful suggestions and discussion on this work; H. Downes and I. Coulson for their constructive reviews.

References

Acocella, V., Puglisi, G., Amelung, F., 2013. Preface - Flank instability at Mt. Etna. Journal of Volcanology and Geothermal Research 251, 1-4.

Allard, P., Behncke, B., D'Amico, S., Neri, M., Gambino, S., 2006. Mount Etna 1993-2005: Anatomy of an evolving eruptive cycle. Earth-Science Reviews 78, 85-114.

Aloisi, M., Cocina, O., Neri, G., Orecchio, B., Privitera, E., 2002. Seismic tomography of the crust underneath the Etna volcano, Sicily. Physics of the Earth and Planetary Interiors 134, 139-155.

Andronico, D., Corsaro, R.A., 2011. Lava fountains during the episodic eruption of South-East Crater (Mt. Etna), 2000: insights into magma-gas dynamics within the shallow volcano plumbing system. Bulletin of Volcanology 73, 1165-1178.

Arevalo, R., Jr., McDonough, W. F., 2010. Chemical variations and regional diversity observed in MORB. Chemical Geology 271, 1-2, 70-85.

Armienti, P., Innocenti, F. Petrini, R., Pompilio, M., Villari, L., 1988. Sub-aphyric alkali basalt from Mt. Etna: Inferences on the depth and composition of the source magma. Rendiconti Società Italiana Mineralogia Petrologia 43, 877– 891.

Armienti, P., Tonarini, S., D'Orazio, M., Innocenti, F., 2004. Genesis and evolution of Mt. Etna alkaline lavas: petrological and Sr-Nd-B isotope constraints. Periodico Di Mineralogia 73, 29-52.

Asimow, P.D., Langmuir, G.H., 2006. The importance of water to oceanic mantle melting regimes. Nature 421, 815-820.

Aurisicchio, C., Scribano, V.,1987. Some ultramafic xenoliths from Etna. Rendiconti Società Italiana Mineralogia Petrologia 42, 219–224.

Azzaro, R., Barbano, M.S., Antichi, B., Rigano, R., 2000. Macroseismic catalogue of Mt. Etna earthquakes from 1832 to 1998. Acta Vulcanologica 12, 1, 3-36 with CD-ROM.

CMTE Working Group, 2014. Catalogo Macrosismico dei Terremoti Etnei, 1832-2013. INGV Catania.http://www.ct.ingv.it/macro/

Beccaluva, L., Bianchini, G., Coltorti, M., 2013. Comments on the paper "A crustal-upper mantle model for southeastern Sicily (Italy) from the integration of petrologic and geophysical data" by Manuella et al. (2013). Journal of Geodynamics 70, 58-60.

Bousquet, J. C., Lanzafame, G.,(2004. The Tectonics and Geodynamics of Mt. Etna: Synthesis and Interpretation of Geological and Geophysical Data. In Mt. Etna: Volcano Laboratory (eds A. Bonaccorso, S. Calvari, M. Coltelli, C. Del Negro and S. Falsaperla), American Geophysical Union, Washington, D. C.. doi: 10.1029/143GM03

Branca, S., Coltelli, M., Groppelli, G., Lentini, F., 2011. Geological map of Etna volcano, 1:50,000 scale. Italian Journal of Geosciences 130, 265-291.

Branca, S., Del Carlo, P.,2004. Eruptions of Mt. Etna During the Past 3,200 Years: a Revised Compilation Integrating the Historical and Stratigraphic Records. In Mt. Etna: Volcano Laboratory (eds A. Bonaccorso, S. Calvari, M. Coltelli, C. Del Negro and S. Falsaperla), American Geophysical Union, Washington, D. C.. doi: 10.1029/143GM02

Carignan, J., Hild, P., Mevelle, G., Morel, J., Yeghicheyan, D., 2001. Routine analyses of trace elements in geological samples using flow injection and low pressure on-line liquid chromatography coupled to ICP-MS: A study of geochemical reference materials BR, DR-N, UB-N, AN-G and GH. Geostandards Newsletter-the Journal of Geostandards and Geoanalysis 25, 187-198.

Clocchiatti, R., Joron, J.L., Treuil, M., 1988. The role of selective alkali contamination in the evolution of recent historic lavas of Mt Etna. Journal of Volcanology and Geothermal Research 34, 241-249.

Clocchiatti, R., Métrich, N., 1986. Refilling and mineralogical disequilibrium in Etnean lava - the Monte Frumento delle Concazze eruption. Comptes Rendus De L Academie Des Sciences Serie Ii 303, 1117-1122.

Collins, S.J., Pyle, D.M., Maclennan, J., 2009. Melt inclusions track pre-eruption storage and dehydration of magmas at Etna. Geology 37, 571-574.

Coltelli, M., Del Carlo, P., Pompilio, M., Vezzoli, L., 2005. Explosive eruption of a picrite: The 3930 BP subplinian eruption of Etna volcano (Italy). Geophysical Research Letters 32.

Condomines, M., Tanguy, J.C., Michaud, V., 1995. Magma dynamics at mt Etna - constraints from U-Th-Ra-Pb radioactive disequilibria and Sr isotopes in historical lavas. Earth and Planetary Science Letters 132, 25-41.

Correale, A., Martelli, M., Paonita, A., Rizzo, A., Brusca, L., Scribano, V., 2012. New evidence of mantle heterogeneity beneath the Hyblean Plateau (southeast Sicily, Italy) as inferred from noble gases and geochemistry of ultramafic xenoliths. Lithos 132, 70-81.

Correale, A., Paonita, A., Martelli, M., Rizzo, A., Rotolo, S.G., Corsaro, R.A., Di Renzo, V., 2014. A two-component mantle source feeding Mt. Etna magmatism: Insights from the geochemistry of primitive magmas. Lithos 184, 243-258.

Correale, A., Paonita, A., Rizzo, A., Grassa, F., Martelli, M., 2015. The carbon-isotope signature of ultramafic xenoliths from the Hyblean Plateau (southeast Sicily, Italy): Evidence of mantle heterogeneity. Geochemistry Geophysics Geosystems 16, 600-611.

Corsaro, R.A., Civetta, L., Di Renzo, V., Miraglia, L., 2009a. Petrology of lavas from the 2004-2005 flank eruption of Mt. Etna, Italy: inferences on the dynamics of magma in the shallow plumbing system. Bulletin of Volcanology 71, 781-793.

Corsaro, R.A., Di Renzo, V., Distefano, S., Miraglia, L., Civetta, L., 2013. Relationship between petrologic processes in the plumbing system of Mt. Etna and the dynamics of the eastern flank from 1995 to 2005. Journal of Volcanology and Geothermal Research 251, 75-89.

Corsaro, R.A., Metrich, N., Allard, P., Andronico, D., Miraglia, L., Fourmentraux, C., 2009b. The 1974 flank eruption of Mount Etna: An archetype for deep dike-fed eruptions at basaltic volcanoes and a milestone in Etna's recent history. Journal of Geophysical Research-Solid Earth 114.

Corsaro, R.A., Miraglia, L., 2014. The transition from summit to flank activity at Mt. Etna, Sicily (Italy): Inferences from the petrology of products erupted in 2007-2009. Journal of Volcanology and Geothermal Research 275, 51-60.

Corsaro, R.A., Miraglia, L., Pompilio, M., 2007. Petrologic evidence of a complex plumbing system feeding the July-August 2001 eruption of Mt. Etna, Sicily, Italy. Bulletin of Volcanology 69, 401-421.

Corsaro, R. A., Pompilio, M., 2004. Dynamics of Magmas at Mount Etna. In Mt. Etna: Volcano Laboratory (eds A. Bonaccorso, S. Calvari, M. Coltelli, C. Del Negro and S. Falsaperla), American Geophysical Union, Washington, D. C.. doi: 10.1029/143GM07.

Corsaro, R.A., Rotolo, S.G., Cocina, O., Tumbarello, G., 2014. Cognate xenoliths in Mt. Etna lavas: witnesses of the high-velocity body beneath the volcano. Bulletin of Volcanology 76.

Coulson, I.M., Stuart, F.M., MacLean, N.J., 2011. Assessing the link between mantle source and sub-volcaninc plumbing in the petrology of basalts from the 2001 and 2002/2003 eruptions of Mount Etna, Sicily: Evidence from geochemical and helium isotope data. Lithos 123, 254-261.

Del Carlo, P., Vezzoli, L., Coltelli, M., 2004. Last 100 Ka Tephrostratigraphic Record of Mount Etna. In Mt. Etna: Volcano Laboratory (eds A. Bonaccorso, S. Calvari, M. Coltelli, C. Del Negro and S. Falsaperla), American Geophysical Union, Washington, D. C.. doi: 10.1029/143GM06

D'Orazio, M., Armienti, P., Cerretini, S., 1998. Phenocryst/matrix trace-element partition coefficients for hawaiite-trachyte lavas from the Ellittico volcanic sequence (Mt. Etna, Sicily, Italy). Mineralogy and Petrology 64, 65-88.

Ferlito, C., Coltorti, M., Cristofolini, R., Giacomoni, P.P., 2009. The contemporaneous emission of low-K and high-K trachybasalts and the role of the NE Rift during the 2002 eruptive event, Mt. Etna, Italy. Bulletin of Volcanology 71, 575-587.

Ferlito, C., Coltorti, M., Lanzafame, G., Giacomoni, P.P., 2014. The volatile flushing triggers eruptions at open conduit volcanoes: Evidence from Mount Etna volcano (Italy). Lithos 184, 447-455.

Ferlito, C., Lanzafame, G., 2010. The role of supercritical fluids in the potassium enrichment of magmas at Mount Etna volcano (Italy). Lithos 119, 642-650.

Goes, S., Giardini, D., Jenny, S., Hollenstein, C., Kahle, H.-G., Geiger, A., 2004. A recent tectonic reorganization in the south-central Mediterranean. Earth and Planetary Science Letters 226, 335–345, doi:10.1016/j.epsl.2004.07.038

Gvirtzman, Z., Nur, A., 1999. The formation of Mount Etna as the consequence of slab rollback. Nature 401, 782-785.

Harris, A., Steffke, A., Calvari, S., Spampinato, L., 2011. Thirty years of satellite ‐ derived lava discharge rates at Etna: Implications for steady volumetric output. Journal of Geophysical Research 116, B08204, doi:10.1029/2011JB008237.

Kahl, M., Chakraborty, S., Costa, F., Pompilio, M., 2011. Dynamic plumbing system beneath volcanoes revealed by kinetic modeling, and the connection to monitoring data: An example from Mt. Etna. Earth and Planetary Science Letters 308, 11–22, doi:10.1016/j.epsl.2011.05.008

Kamenetsky, V., Clocchiatti, R., 1996. Primitive magmatism of Mt Etna: Insights from mineralogy and melt inclusions. Earth and Planetary Science Letters 142, 553-572.

Kamenetsky, V.S., Pompilio, M., Metrich, N., Sobolev, A.V., Kuzmin, D.V., Thomas, R., 2007. Arrival of extremely volatile-rich high-Mg magmas changes explosivity of Mount Etna. Geology 35, 255-258.

Lo Giudice, A., Rittmann, L., 1975. Su alcune accumuliti etnee: aspetti mineralogici e genetici. Rivista Mineraria Siciliana 26, 1–12.

Manuella, F.C., Brancato, A., Carbone, S., Gresta, S., 2013. A crustal-upper mantle model for southeastern Sicily (Italy) from the integration of petrologic and geophysical data. Journal of Geodynamics 66, 92-102.

Manuella, F.C., Brancato, A., Carbone, S., Gresta, S., 2014. Reply to "Comments on the paper "A crustal-upper mantle model for southeastern Sicily (Italy) from the integration of petrologic and geophysical data" by Manuella et al. (2013)". Journal of Geodynamics 73, 81-82.

Marty, B., Trull, T., Lussiez, P., Basile, I., Tanguy, J.C., 1994. He, Ar, O, Sr AND Nd isotope constraints on the origin and evolution of Mount Etna magmatism. Earth and Planetary Science Letters 126, 23-39.

Métrich, N., Allard, P., Spilliaert, N., Andronico, D., Burton, M., 2004. 2001 flank eruption of the alkali- and volatile-rich primitive basalt responsible for Mount Etna's evolution in the last three decades. Earth and Planetary Science Letters 228, 1-17.

Monaco,C., Catalano, S., Cocina,O., De Guidia, G., Ferlito, C., Gresta, S., Musumeci, C., Tortoricia, L., 2005. Tectonic control on the eruptive dynamics at Mt. Etna Volcano (Sicily) during the 2001 and 2002–2003 eruptions. Journal of Volcanology and Geothermal Research 144, 211 – 233

Patanè, D., Barberi, G., Cocina, O., De Gori, P., Chiarabba, C., 2006. Timeresolved seismic tomography detects magma intrusions at Mount Etna. Science 313, 821–823. doi:10.1126/science.1127724

Ruscitto, D. M., Wallace, P. J., Cooper, L. B., Plank, T., 2012. Global variation in H_2O/Ce: 2. Relationships to arc magma geochemistry and volatile fluxes. Geochimistry Geophysics Geosystems13(3), doi:10.1029/2011GC003887.

Salters, V.J.M., Stracke, A., 2004. Composition of the depleted mantle. Geochemistry Geophysics Geosystems 5.

Sapienza, G., Scribano, V., 2000. Distribution and representative whole rock chemistry of deep-seated xenoliths from the Iblean Plateau, South-Eastern Sicily, Italy. Periodico di Mineralogia 69, 185–204.

Schiano, P., Clocchiatti, R., Ottolini, L., Busa, T., 2001. Transition of Mount Etna lavas from

a mantle-plume to an island-arc magmatic source. Nature 412, 900-904.

Scribano, V., Sapienza, G.T., Braga R., Morten,, L. 2006. Gabbroic xenoliths in tuff-breccia pipes from the Hyblean plateau: insights into the nature and composition of the lower crust underneath South-Eastern Sicily, Italy. Mineralogy and Petrology, 86, 63-88.

Shaw, D.M., 1970. Trace element fractionation during anatexis. Geochimica Et Cosmochimica Acta 34, 237-243.

Sorbadere, F., Schiano, P., Métrich, N. 2013. Constraints on the origin of nepheline-normative primitive magmas in island arcs. Journal of Petrology 54/2, 215-233, doi: 10.1093/petrology/egs063.

Spilliaert, N., Allard, P., Métrich, N., Sobolev, A.V., 2006. Melt inclusion record of the conditions of ascent, degassing, and extrusion of volatile-rich alkali basalt during the powerful 2002 flank eruption of Mount Etna (Italy). Journal of Geophysical Research-Solid Earth 111.

Stracke, A., Bizimis, M., Salters, V.J.M., 2003. Recycling oceanic crust: Quantitative constraints. Geochemistry Geophysics Geosystems 4.

Suiting, I., Schmincke H.U., 2010. Hyblean diatremes 2: shallow marine volcanism in the central mediterranean at the onset of the Messinian salinity crisis (Hyblean mountains, SE-Sicily) - a multidisciplinary approach. International. Journal. Earth Science. (Geol. Rundschau), 99, 1917-1940.

Tanguy J. C. (1980) L'Etna: étude pétrologique et paléomagnetique : implications volcanologiques. Thèse d'Etat. Paris VI, 618 pp.

Tatsumi, Y., 1989. Migration of fluid phases and genesis of basalt magmas in subduction zones: Journal of Geophysical Research 94, 4697-4707.

Tonarini, S., Armienti, P., D'Orazio, M., Innocenti, F., 2001. Subduction-like fluids in the genesis of Mt. Etna magmas: evidence from boron isotopes and fluid mobile elements. Earth and Planetary Science Letters 192, 471-483.

Trua, T., Esperanca, S., Mazzuoli, R., 1998. The evolution of the lithospheric mantle along the N African Plate: geochemical and isotopic evidence from the tholeiitic and alkaline volcanic rocks of the Hyblean Plateau, Italy. Contributions to Mineralogy and Petrology 131, 307-322.

Viccaro, M., Cristofolini, R., 2008. Nature of mantle heterogeneity and its role in the short-term geochemical and volcanological evolution of Mt. Etna (Italy). Lithos 105, 272-288.

Viccaro, M., Giacomoni, P.P., Ferlito, C., Cristofolini, R., 2008. A new perspective on the geochemical signature of Mt. Etna alkaline magmas. Geochimica et Cosmochimica Acta 72,

A982-A982.

Table1

Bulk rock major and trace elements in lava flows of Mt. Frumento delle Concazze, Mt. Spagnolo and Mt. Maletto eruptions and in tephra from the FS eruption. Sample FDC2c is a scoria sample of the Mt. Frumento delle Concazze pyroclastic cone.

Table 2

Electron microprobe analyses of the major element, S and Cl contents of olivine-hosted melt inclusions and matrix glasses of Mt Etna samples

Figure captions

Figure 1

a) Digital Elevation Model of Mt. Etna with the location of the studied *DDF* eruptions of Mongibello (15 ka-present); eruptions occurring in historic times are indicated in red. In b), c) and d) are drawn, respectively, the lava flow fields of Mt. Maletto, Mt. Spagnolo and Mt. Frumento delle Concazze eruptions (modified from Branca et al., 2011), as well as the location of the sampled lavas (red circle) and pyroclasts (white circle).

Figure 2

Major element concentrations of bulk rocks representative of Etnean magmas emplaced during *DDF* eruptions. MFR, MSP and MAL refer, respectively, to Mts. Frumento delle Concazze, Spagnolo and Maletto. MFR samples which contain plagioclase phenocrysts (symbol: full black square) are distinguished from plagioclase-free samples (symbol: open black square). The black arrows labelled FC describe the evolution of the parent MFR primitive magma (average of basalts MFR5 and MFR6) for the fractional crystallization of 14% solid consisting of 2% plagioclase, 4% olivine and 8% clinopyroxene. For details see Section 3.

Figure 3

Projection from Ol onto the Ne-Di-Qz face of the Ne-Di-Qz-Ol system of major element compositions of Etna *DDF* magmas, after recast of analyses in terms of CMAS components following Sorbadere et al. (2013).

Figure 4

Selected trace element concentrations of bulk basaltic rocks representative of Etnean *DDF* magmas. For the meaning of the FC black arrows, see caption of Fig.2.

Figure 5

Global MORB normalized trace-element patterns for average compositions of Etna *DDF* basalts. Data for MORB are from Arevalo and McDonough (2010).

Figure 6

Variation of Cl and K_2O in olivine-hosted melt inclusions of Etna samples: (a) basalts emplaced during *DDF* eruptions, and (b) trachybasalts magmas emitted during Strombolian and lava fountains at the summit craters North-East (NEC) and Voragine (VOR). Literature data are from [1] Schiano et al. (2001); [2] Spilliaert et al. (2006); [3] Métrich et al. (2004); [4] Corsaro et al. (2009); [5] Collins et al. (2009).

Figure 7

a) Ce/Y vs. Zr/Nb of Etnean *DDF* basalts. Curves of non-modal fractional melting (dashed lines) and accumulated fractional melting (continuous lines) are plotted for three Hyblean-type mantle sources: anhydrous spinel lherzolite (type 1, blue curves), spinel peridotite (type 2; purple curves); a mixture of Hyblean mantle 1-type and clinopyroxenite (black curves). The mineralogical compositions and the source data are given in the text. Ticks indicate the percentages of melting. The curves of fractional melting for depleted garnet and spinel mantles are provided for comparison (dotted black lines). Data for DDM are from Stracke et al. (2003).

b) Enlargement of the boxed area in Figure 7a, showing exclusively the curves for accumulated fractional melting of Hyblean-type mantle sources, with dotted isolines of melting percentages. The average composition ($\pm 1\sigma$) of Miocene Hyblean basalts carrying the mantle xenoliths, which were used for modelling, is given for comparison (data from Scribano et al., 2006; Suiting and Schmincke, 2010).

Figure 8

Selected trace element ratios as a function of Ta/Yb (a) and Sr-isotopic compositions (b) of bulk *DDF* basalts. In Fig. 8a, literature data for flank and summit activity of the period 1995-2009 are from: Andronico and Corsaro (2011); Corsaro and Miraglia (2014); Corsaro et al. (2009, 2013). [1] refers to the Sr isotopic composition of one sample of the 1974 lava

(Armienti et al., 2004). The blue star indicates Ta/Yb=0.05 for N-MORB of Arevalo and McDonough (2010). In Fig. 8b, the dashed line underlines the co-variation of Rb and ^{87}Sr in most *DDF* magmas, with the exception of the post-1970s Etna basalts which depart (see the arrow) from the general trend in being selectively enriched in Rb. Sr isotope data are from Correale et al. (2014), Corsaro et al. (2009), Di Renzo, unpublished data, [1] Armienti et al. (2004).

Figure 9

Variation of Cl and Na_2O in Etna melt inclusions normalized to K_2O. We plot the average values of the Na_2O/K_2O and Cl/K_2O ratios for each *DDF* basalt. The number of analyses which has been averaged is given in parenthesis: MFR (8), FS (8); 2002-03 (157); 2001 (10); 1763 (14). For MFR and FS tephra the data are new, as those for the 1995-2009 period of activity. Literature data are: [MAL] from Schiano et al., (2001); [2002] from Spilliaert et al., (2006); [2001] from Métrich et al., (2004); [1763 and 1974] from Corsaro et al., (2009).

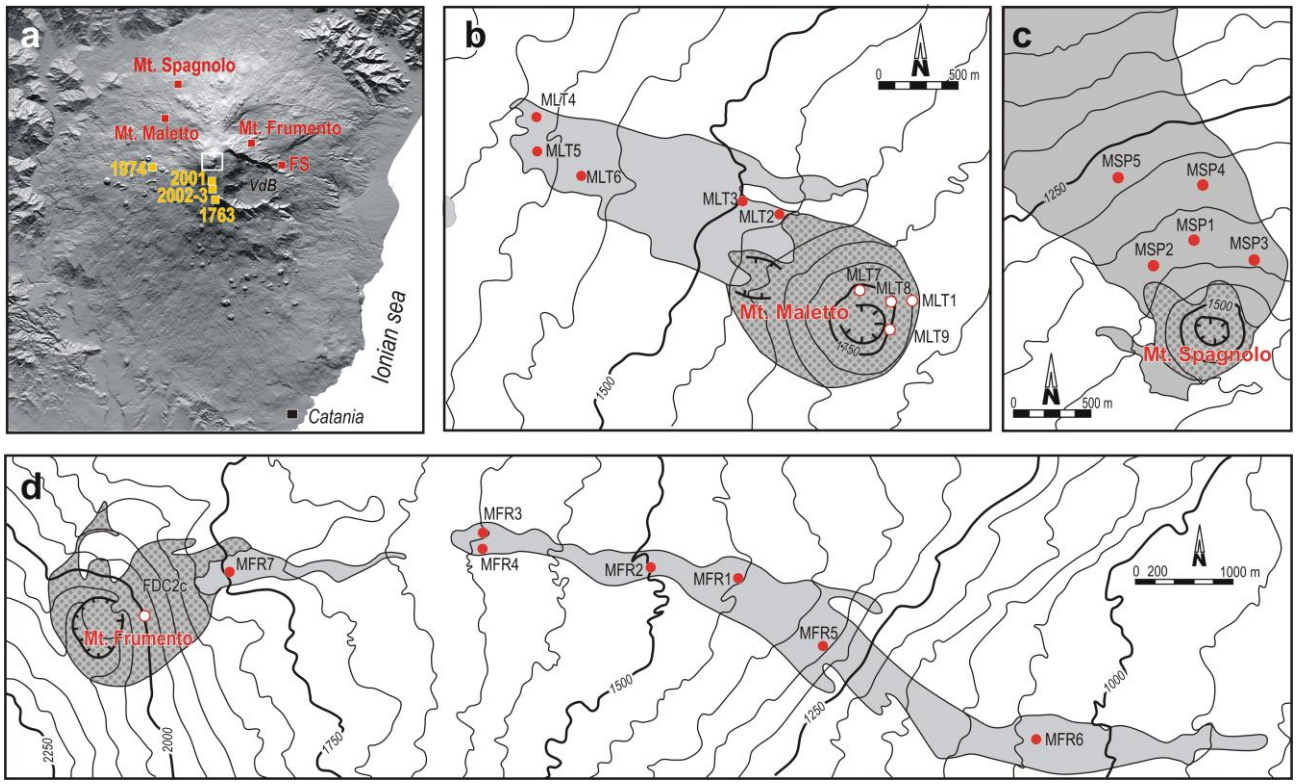

Figure 1

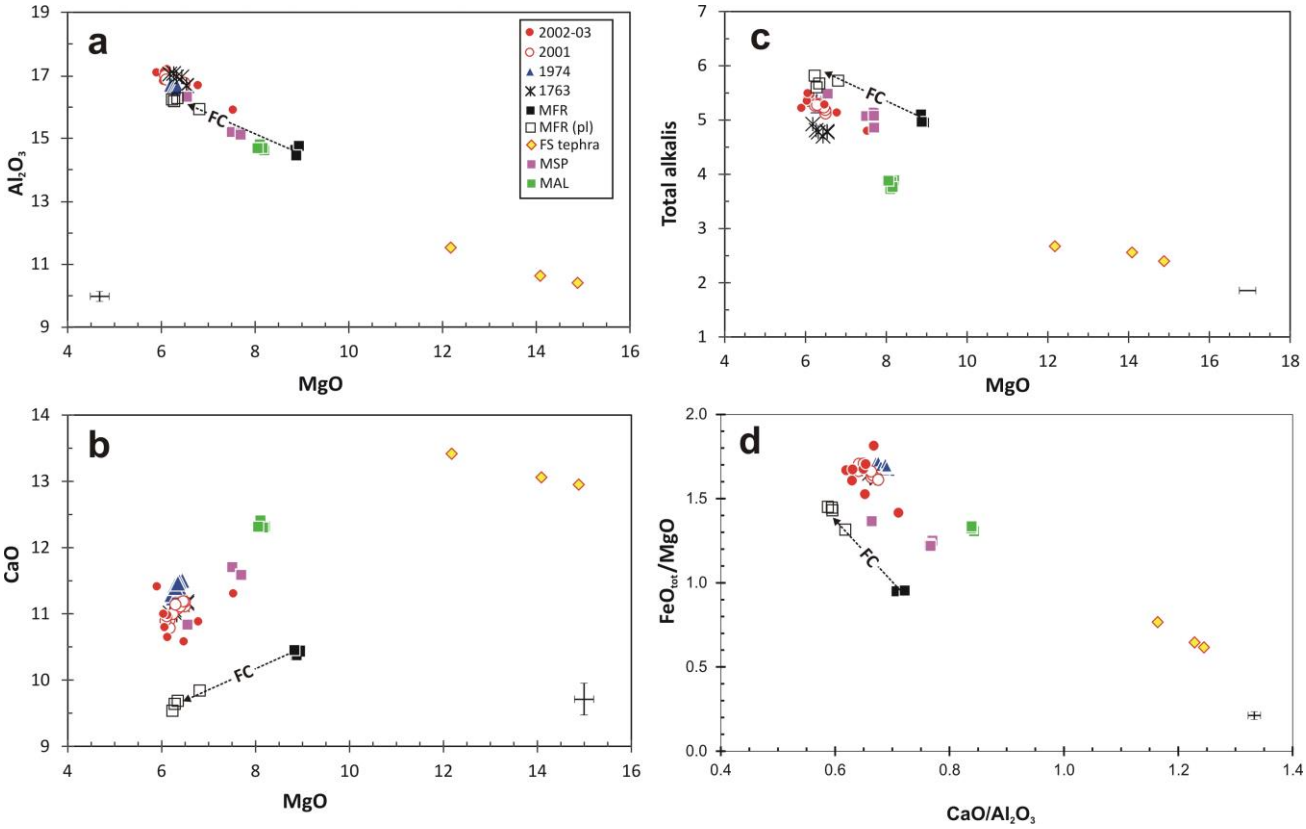

Figure 2

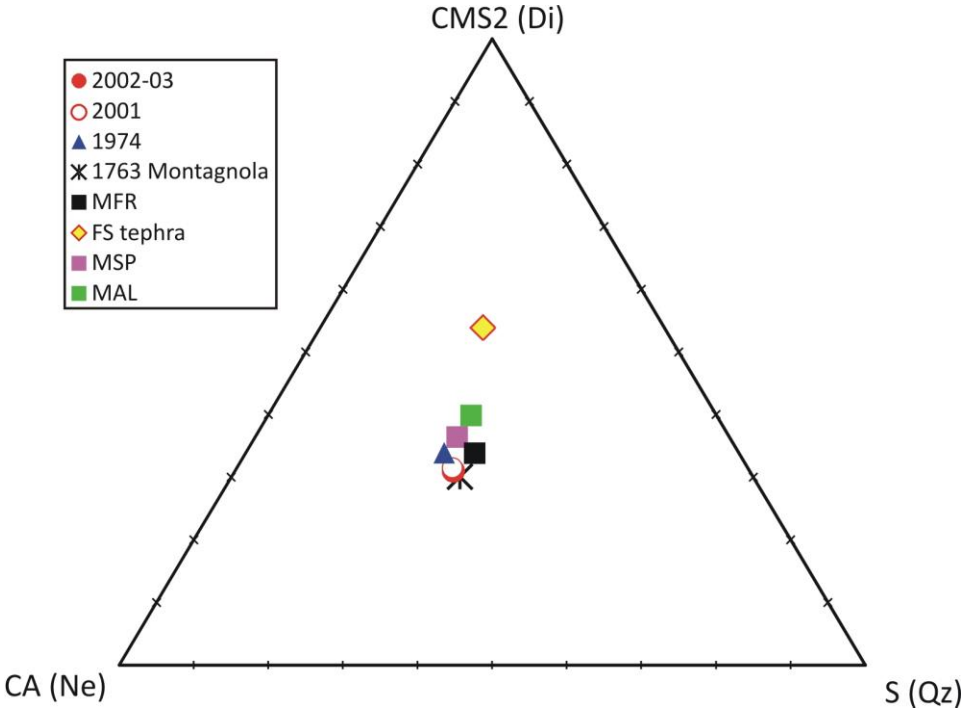

Figure 3

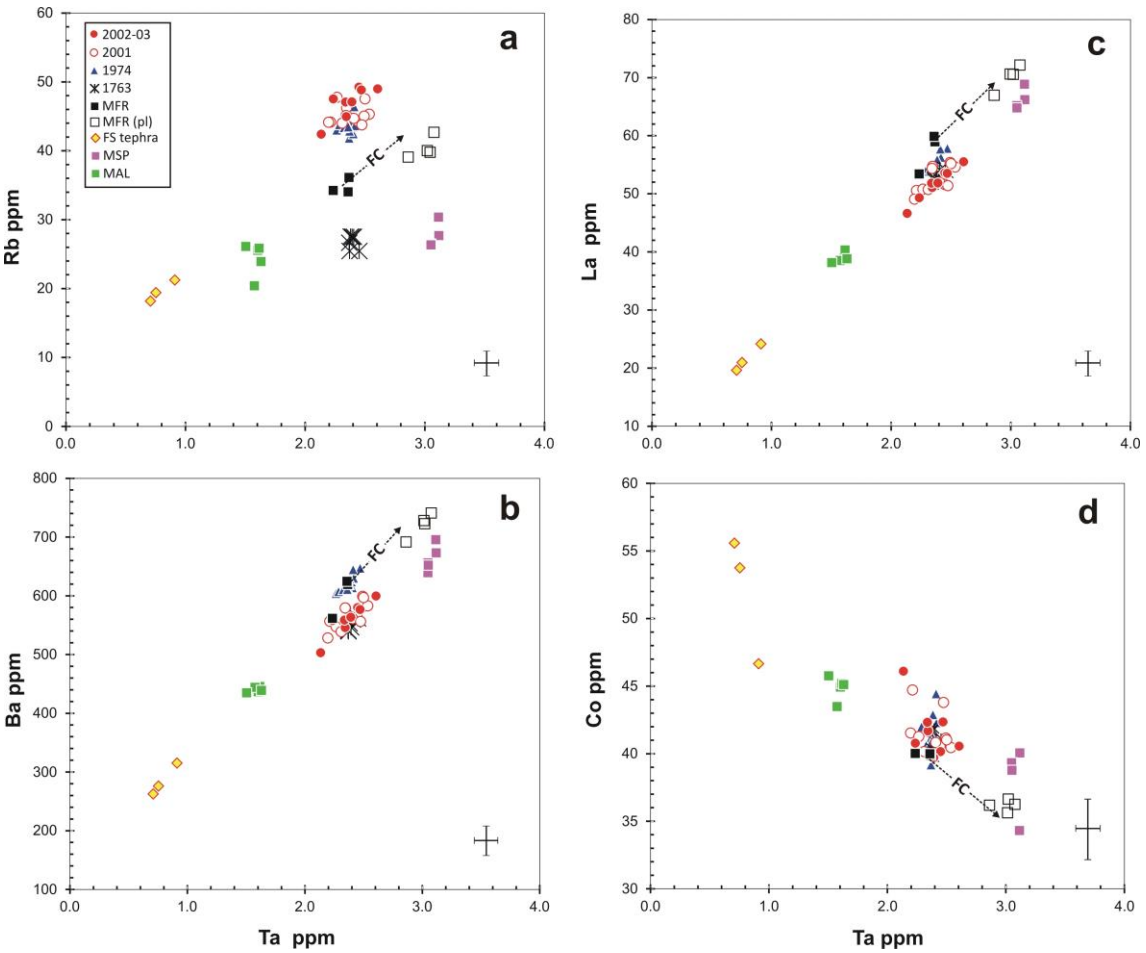

Figure 4

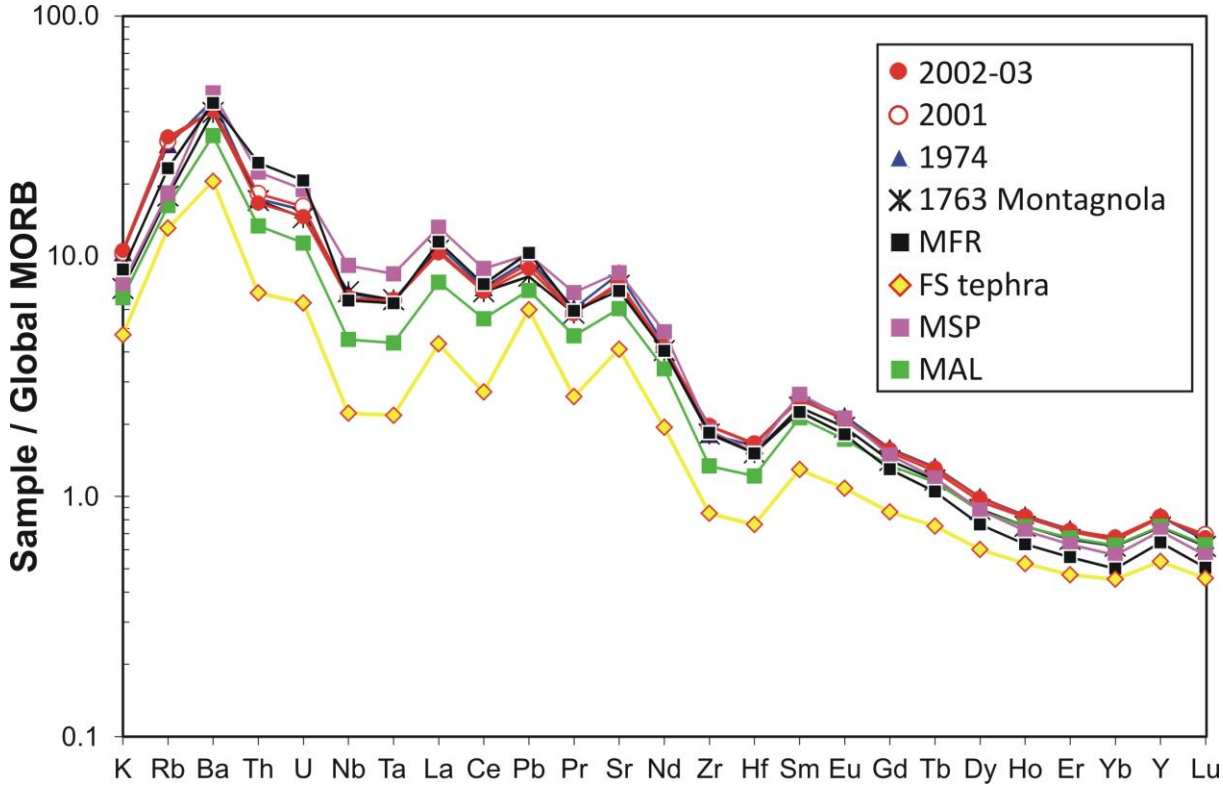
100.0
10.0
1.0
0.1
Sample / Global MORB
2002-03
2001
1974
1763 Montagnola
MFR
FS tephra
MSP
MAL
K Rb Ba Th U Nb Ta La Ce Pb Pr Sr Nd Zr Hf Sm Eu Gd Tb Dy Ho Er Yb Y Lu

Figure 5

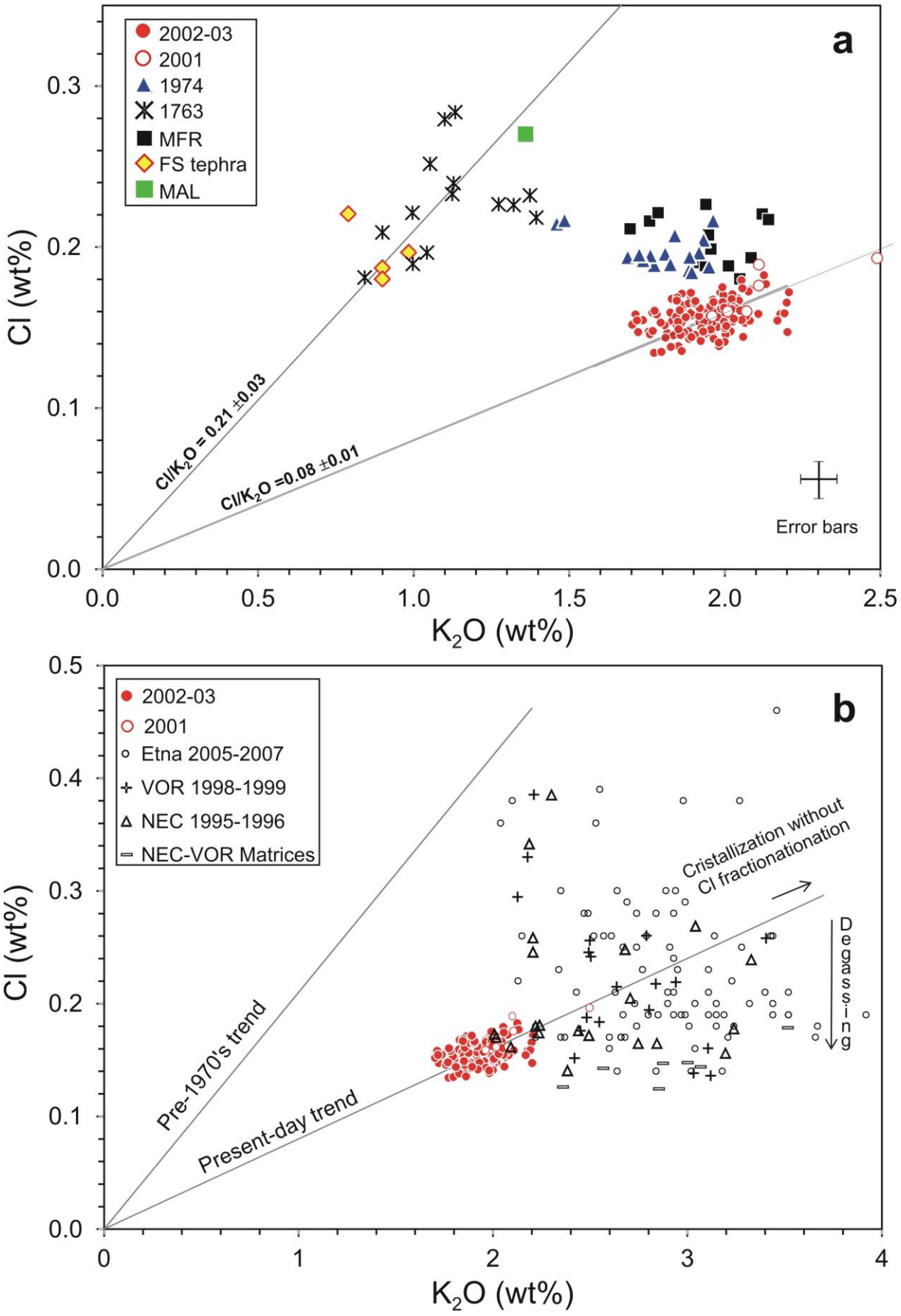
a
2002-03
2001
1974
1763
MFR
FS tephra
MAL
Cl/K2O = 0.21 ±0.03
Cl/K2O =0.08 ±0.01
Error bars
Cl (wt%)
K2O (wt%)
b
2002-03
2001
Etna 2005-2007
VOR 1998-1999
NEC 1995-1996
NEC-VOR Matrices
Cristallization without Cl fractionation
Degassing
Pre-1970's trend
Present-day trend
Cl (wt%)
K2O (wt%)

Figure 6

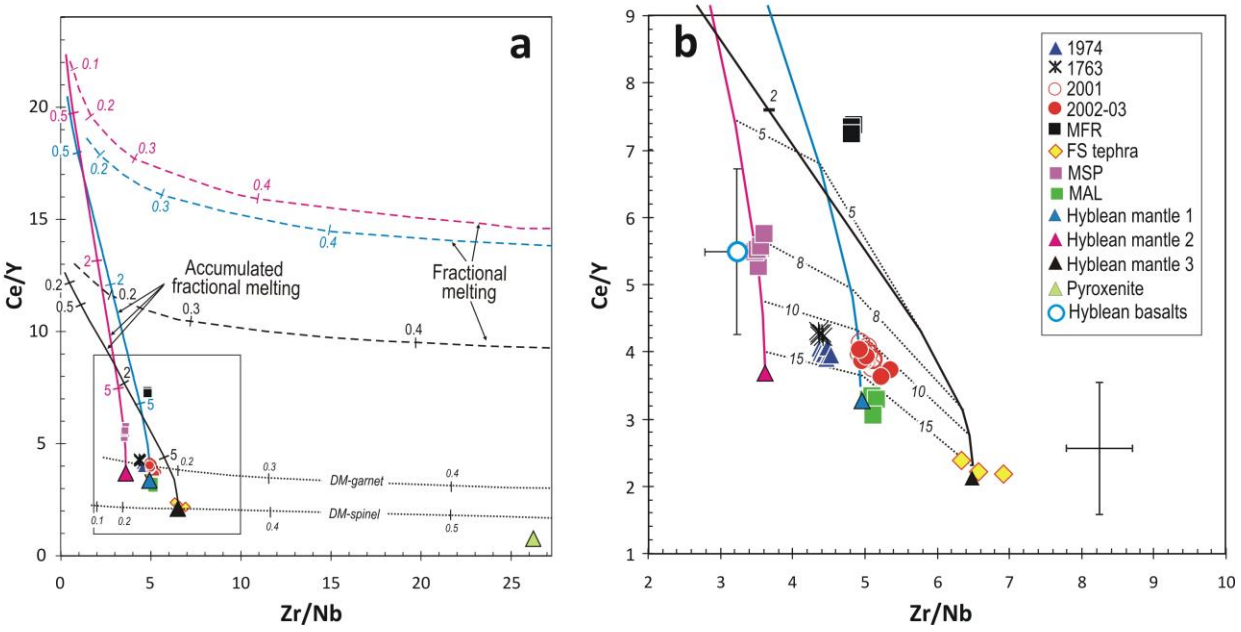

Figure 7

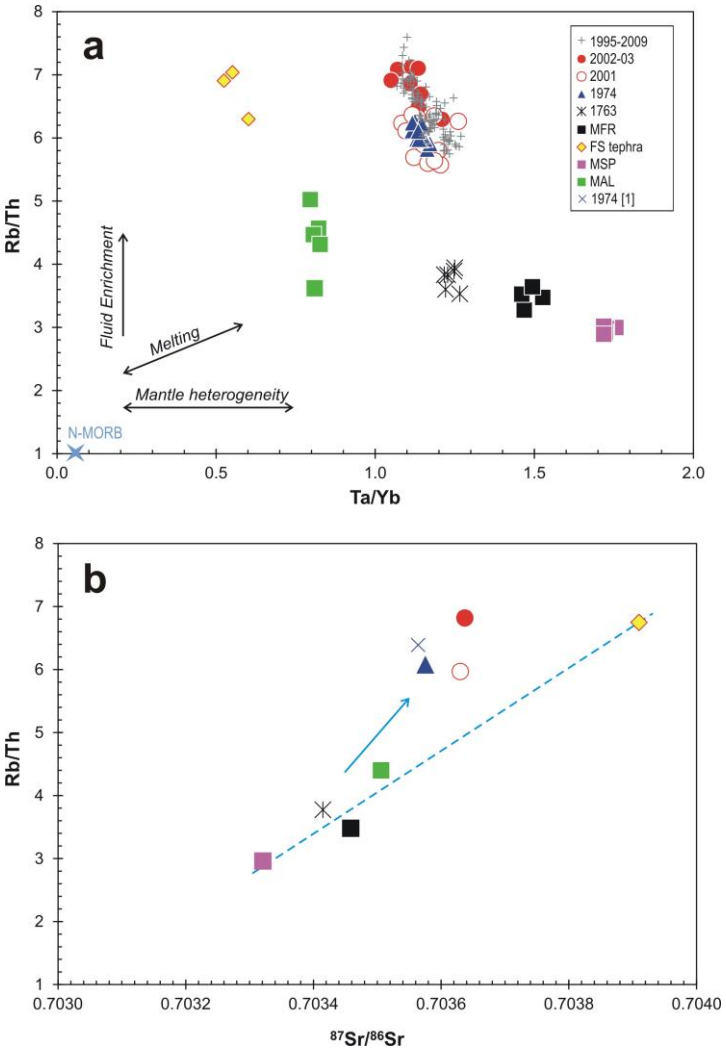

Figure 8

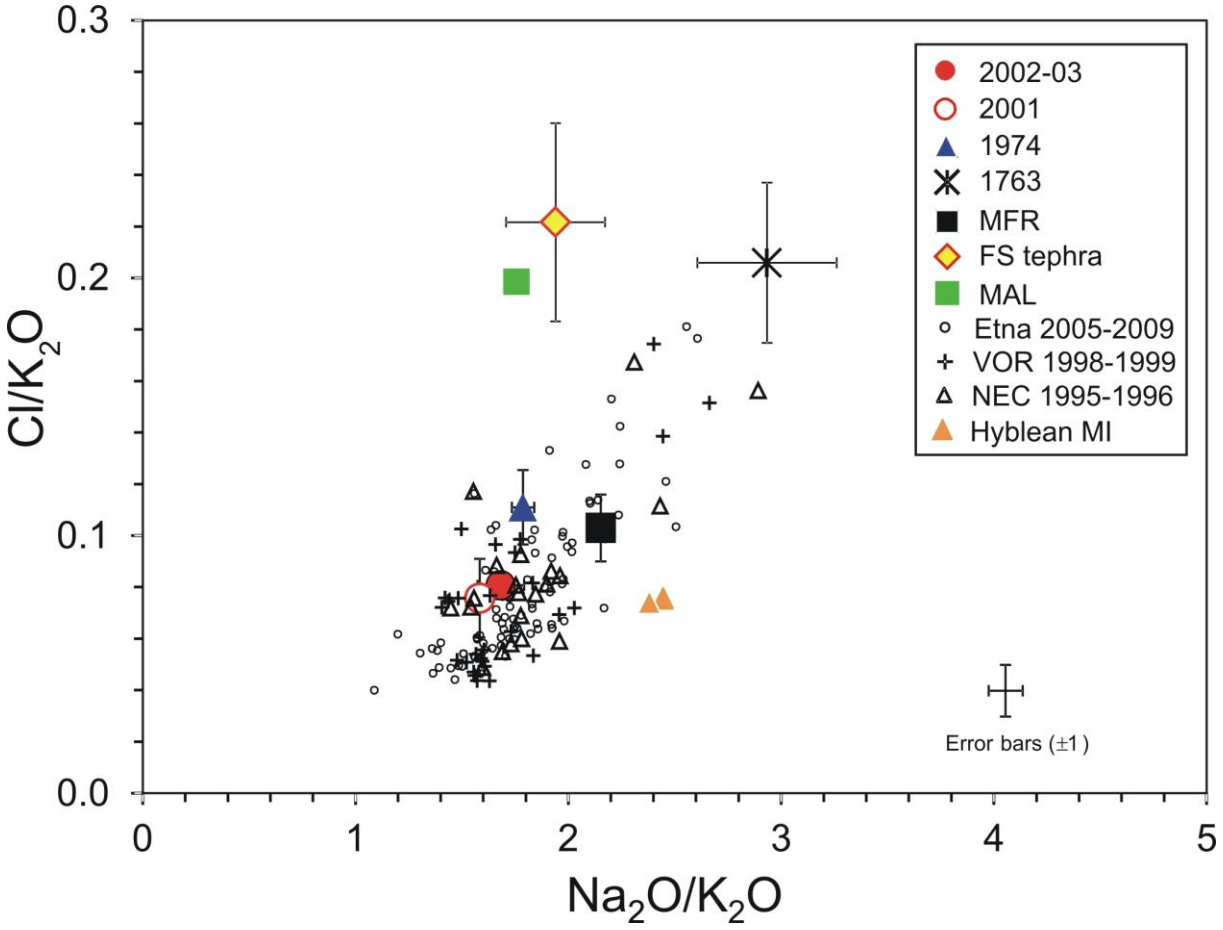
0.3
0.2
0.1
0.0
Cl/K2O
0
1
2
3
4
5
Na2O/K2O
2002-03
2001
1974
1763
MFR
FS tephra
MAL
Etna 2005-2009
VOR 1998-1999
NEC 1995-1996
Hyblean MI
Error bars (±1)

Figure 9

Table 1

	MT. FRUMENTO DELLE CONCAZZE								FS TEPHRA			MT. SPAGNOLO					MT. MALETTO				
sample	***MFR1***	***MFR2***	***MFR3***	***MFR4***	***MFR5***	***MFR6***	***MFR7***	***FDC2c***	***FS2***	***FS8***	***FS7***	***MSP1***	***MSP2***	***MSP3***	***MSP4***	***MSP5***	***MLT2***	***MLT3***	***MLT4***	***MLT5***	***MLT6***
SiO_2	50.16	50.12	50.45	50.50	50.37	49.82	50.64	49.74	47.61	47.11	48.46	48.36	47.64	48.46	48.38	47.69	47.85	47.45	47.47	47.64	47.93
TiO_2	1.45	1.41	1.47	1.47	1.28	1.30	1.26	1.41	0.92	0.90	1.01	1.51	1.49	1.52	1.44	1.47	1.49	1.50	1.51	1.51	1.51
Al_2O_3	16.14	15.83	16.14	16.13	14.58	14.62	14.41	15.40	10.49	10.23	11.54	15.11	14.82	15.15	15.98	14.81	14.57	14.57	14.71	14.59	14.66
Fe_2O_3	10.00	9.90	9.99	10.03	9.29	9.34	9.38	9.93	9.95	10.00	10.36	10.36	10.30	10.45	9.73	10.22	11.86	11.84	11.98	11.92	11.94
MnO	0.16	0.16	0.16	0.16	0.15	0.15	0.15	0.16	0.18	0.18	0.18	0.16	0.16	0.17	0.16	0.16	0.19	0.19	0.19	0.19	0.19
MgO	6.29	6.77	6.19	6.25	8.83	8.85	8.86	7.50	13.90	14.64	12.19	7.46	7.53	7.68	6.41	7.54	8.18	8.05	8.05	8.10	8.04
CaO	9.61	9.79	9.48	9.59	10.38	10.34	10.40	10.23	12.89	12.74	13.43	11.64	11.34	11.58	10.61	11.36	12.29	12.23	12.33	12.22	12.30
Na_2O	3.79	3.88	3.85	3.66	3.45	3.30	3.37	3.58	1.66	1.57	1.75	3.69	3.40	3.75	3.82	3.60	2.63	2.58	2.52	2.54	2.60
K_2O	1.84	1.82	1.94	1.91	1.64	1.61	1.59	1.70	0.86	0.79	0.93	1.36	1.35	1.39	1.55	1.38	1.25	1.24	1.18	1.20	1.27
P_2O_5	0.61	0.60	0.62	0.63	0.50	0.53	0.47	0.58	0.24	0.23	0.27	0.66	0.66	0.65	0.68	0.66	0.42	0.43	0.44	0.43	0.43
L.O.I.	0.25	-0.21	-0.11	0.09	-0.05	0.74	-0.19	0.44	0.32	0.40	0.89	-0.08	0.62	-0.04	0.12	0.15	-0.29	0.20	0.19	0.09	-0.29
TOT	100.31	100.06	100.18	100.43	100.41	100.60	100.33	100.67	99.02	98.81	101.00	100.21	99.32	100.74	98.87	99.03	100.44	100.28	100.56	100.42	100.58
Rb	40.0	39.1	42.7	39.9	36.1	34.0	34.2	36.8	19.4	18.2	21.2	26.6	27.7	26.5	30.4	26.3	25.6	25.9	20.4	23.9	26.1
Cs	0.67	0.86	0.89	0.79	0.66	0.58	0.76	0.91	0.47	0.45	0.56	0.55	0.53	0.54	0.61	0.54	0.50	0.58	0.34	0.40	0.49
Ba	723	692	741	728	619	624	562	730	276	262	315	639	673	656	696	652	437	446	444	439	435
Th	13.0	12.3	13.4	13.1	10.4	10.4	9.7	10.1	2.8	2.6	3.4	8.9	9.3	9.1	10.1	9.1	5.6	5.8	5.6	5.5	5.2
U	3.53	3.47	3.51	3.52	2.93	2.90	2.66	3.15	0.83	0.80	0.99	2.50	2.55	2.55	2.83	2.56	1.62	1.68	1.36	1.61	1.51
Nb	51.0	47.8	51.6	51.5	38.6	39.3	36.3	46.7	12.6	11.5	14.7	53.3	54.6	52.8	53.3	52.0	26.1	26.4	25.9	26.0	26.6
Ta	3.02	2.86	3.08	3.02	2.37	2.36	2.24	2.70	0.75	0.71	0.91	3.05	3.12	3.05	3.12	3.05	1.60	1.62	1.58	1.63	1.50
La	70.5	66.9	72.2	70.3	59.0	59.9	53.4	72.3	21.0	19.6	24.2	64.8	66.2	65.2	68.9	64.8	38.9	40.3	38.5	38.8	38.2
Ce	129	124	132	129	109	112	100	126	37	35	42	120	126	123	130	123	77	79	77	77	74
Pb	8.04	7.98	8.79	8.65	7.29	6.76	6.65	8.10	4.09	3.60	4.30	6.21	6.16	6.15	7.35	8.14	5.09	5.16	5.02	3.85	4.93
Pr	14.06	13.33	14.26	14.05	12.10	12.35	11.04	13.95	5.02	4.85	5.76	13.74	14.29	14.10	14.51	13.95	9.35	9.63	9.36	9.35	8.92
Sr	1067	1036	1052	1042	1026	1038	947	1012	569	546	607	1211	1187	1179	1231	1169	841	853	837	839	859
Nd	50.8	48.6	52.0	51.3	45.0	46.0	40.9	51.1	20.4	19.8	23.2	52.9	53.1	52.8	53.2	51.7	37.1	37.6	37.2	37.4	36.0
Zr	217	206	223	219	187	189	175	202	83	79	93	188	190	185	192	185	132	135	132	134	136
Hf	4.61	4.42	4.77	4.60	4.04	4.06	3.86	4.32	1.98	1.87	2.20	3.90	4.15	3.96	4.13	4.00	3.28	3.26	3.21	3.21	3.09
Sm	8.97	8.63	9.13	8.98	7.98	8.15	7.37	8.73	4.38	4.26	4.91	9.16	9.36	9.42	9.29	9.21	7.44	7.55	7.37	7.47	7.23
Eu	2.56	2.45	2.55	2.54	2.36	2.40	2.20	2.56	1.34	1.33	1.49	2.70	2.75	2.73	2.70	2.68	2.23	2.23	2.21	2.22	2.17
Gd	6.76	6.51	6.91	6.73	6.16	6.23	5.66	6.86	3.90	3.78	4.30	6.87	7.11	6.85	6.88	6.82	6.23	6.35	6.27	6.27	6.07
Tb	0.90	0.86	0.91	0.90	0.82	0.81	0.77	0.90	0.55	0.55	0.62	0.91	0.93	0.91	0.90	0.90	0.87	0.88	0.89	0.88	0.85
Dy	4.58	4.45	4.69	4.65	4.14	4.16	3.91	4.62	3.12	3.07	3.42	4.56	4.75	4.71	4.68	4.66	4.65	4.74	4.65	4.65	4.50
Ho	0.80	0.77	0.81	0.81	0.71	0.72	0.68	0.80	0.57	0.56	0.63	0.79	0.81	0.79	0.80	0.80	0.83	0.84	0.83	0.84	0.81
Er	2.09	2.01	2.14	2.10	1.86	1.89	1.76	2.06	1.51	1.50	1.65	2.05	2.10	2.09	2.08	2.06	2.22	2.23	2.19	2.25	2.15
Yb	1.85	1.78	1.91	1.87	1.55	1.61	1.53	1.81	1.37	1.35	1.52	1.74	1.81	1.77	1.81	1.78	1.95	2.01	1.95	1.97	1.89
Lu	0.29	0.27	0.28	0.29	0.24	0.24	0.23	0.27	0.21	0.21	0.23	0.26	0.27	0.27	0.27	0.26	0.30	0.30	0.29	0.30	0.29
Y	23.3	22.3	23.5	22.9	20.6	20.8	19.1	23.7	16.6	16.2	17.7	22.8	22.9	22.4	22.5	22.1	23.3	23.7	23.1	23.5	24.1
Ni	55.3	64.0	51.4	50.9	121.5	120.4	118.6	73.4	193.1	214.5	124.6	62.7	66.2	65.2	52.6	64.8	56.9	57.0	54.4	57.4	57.0
Cr	165	196	144	149	461	416	452	251	1093	1228	849	213	231	215	178	224	209	207	192	195	188
V	231	231	240	243	221	199	223	229	230	229	228	267	251	263	239	258	302	301	298	308	312
Co	37	36	36	36	40	40	40	37	54	56	47	39	40	39	34	39	45	45	43	45	46
Cu	109	118	127	111	95	91	106	133	85	88	98	120	111	106	117	105	117	144	118	88	129

Table 2 . Electron microprobe analyses of the major element, S and Cl contents of olivine-hosted melt inclusions and matrix glasses of Mt Etna samples

Sample		Fo (mol%) [1]	SiO_2 (wt%)	TiO_2 (wt%)	Al_2O_3 (wt%)	FeO (wt%)	MgO (wt%)	CaO (wt%)	Na_2O (wt%)	K_2O (wt%)	P_2O_5 (wt%)	S (wt%)	Cl (wt%)	Total (wt%)	Na_2O/K_2O	Cl/K_2O	CaO/Al_2O_3
Monte Frumento delle Concazze - MFR 2b sample																	
MI 20	MI [2]	88.6	49.78	1.25	15.02	6.22	4.98	10.83	3.96	1.76	0.52	0.168	0.216	94.71	0.44	0.123	0.72
MI 22	MI	88.9	51.47	1.33	16.59	5.54	4.30	11.12	4.45	2.12	0.58	0.153	0.221	97.86	0.48	0.104	0.67
MI 11	MI	88.9	51.38	1.18	14.91	5.88	4.90	10.09	3.95	1.90	0.43	0.142	0.190	94.96	0.48	0.100	0.68
MI 9	MI	87.5	52.40	1.23	15.95	6.15	4.52	9.73	4.03	2.05	0.43	0.134	0.180	96.81	0.51	0.088	0.61
MI 7	MI	88.6	52.60	1.20	16.08	5.33	4.37	10.11	4.22	2.08	0.44	0.138	0.193	96.76	0.49	0.093	0.63
MI 17	MI	88.4	51.57	1.38	16.02	5.63	4.18	10.88	4.22	1.96	0.47	0.142	0.199	96.64	0.46	0.102	0.68
MI 17	MI	88.4	52.18	1.33	16.26	5.57	4.18	10.60	4.16	1.94	0.46	0.133	0.188	96.99	0.47	0.097	0.65
MI 37b	MI	88.5	51.43	1.26	16.20	5.77	5.67	10.42	3.88	2.01	0.46	0.144	0.188	97.44	0.52	0.094	0.64
MI 37b	MI	88.5	51.91	1.25	15.55	6.21	4.53	10.64	4.18	1.95	0.43	0.122	0.208	96.97	0.47	0.107	0.68
MI 42a	MI	87.8	50.87	1.39	14.86	5.88	5.10	10.27	3.47	1.70	0.50	0.155	0.211	94.40	0.49	0.125	0.69
MI 42b	MI	87.8	51.06	1.49	15.46	5.88	4.99	10.54	3.84	1.79	0.50	0.155	0.221	95.93	0.47	0.124	0.68
MI 49	MI	*88.5*	50.46	1.65	17.91	4.83	4.11	9.39	4.38	2.14	0.76	0.179	0.217	96.03	0.49	0.101	0.52
MI 26	MI	87.9	48.84	1.41	15.53	7.30	4.97	10.79	4.11	1.67	0.39	0.222	0.226	95.44	0.41	0.135	0.69
MI 21	MI	88.3	48.93	1.48	15.81	6.18	4.86	11.71	4.25	1.89	0.62	0.258	0.271	96.26	0.44	0.144	0.74
MI 15	MI	88.2	48.51	1.47	15.73	6.45	4.87	11.73	4.01	1.76	0.62	0.258	0.254	95.65	0.44	0.144	0.75
MI 4a	MI	89.1	49.08	1.49	15.32	6.40	5.14	11.76	4.01	1.76	0.65	0.300	0.291	96.20	0.44	0.166	0.77
MI 28	MI	87.3	48.34	1.44	15.69	6.71	5.02	11.58	3.87	1.70	0.61	0.260	0.242	95.44	0.44	0.142	0.74
MI 36	MI	88.1	48.16	1.43	15.97	6.63	5.24	11.65	4.12	1.70	0.65	0.268	0.258	96.06	0.41	0.152	0.73
3930 BP (FS) tephra																	
FS06-ol 20	MI	na	48.17	0.91	10.77	8.15	6.50	15.13	1.78	0.90	0.24	0.234	0.187	92.96	1.98	0.21	1.40
FS06-ol 24	MI	na	47.82	0.99	11.10	8.29	5.98	15.84	1.74	0.85	0.30	0.272	0.201	93.37	2.04	0.24	1.43
FS06-ol 31	MI	na	47.48	0.90	10.56	8.18	9.09	13.80	1.60	0.90	0.24	0.241	0.180	93.19	1.78	0.20	1.31
FS06-ol 35	MI	na	47.77	0.92	10.54	8.27	9.10	13.89	1.69	0.93	0.27	0.239	0.176	93.79	1.82	0.19	1.32
FS06-ol 36	MI	na	46.92	0.98	11.21	8.33	9.05	13.91	1.74	0.79	0.28	0.224	0.171	93.60	2.19	0.22	1.24
FS06-ol 37	MI	na	47.48	0.95	11.06	8.24	8.60	13.88	1.68	1.19	0.32	0.224	0.137	93.76	1.41	0.11	1.26
FS06-ol 38	MI	na	47.90	0.97	10.95	8.31	8.43	13.99	1.63	0.78	0.30	0.236	0.159	93.66	2.09	0.20	1.28
Fs06-40	MI	90.5	47.21	0.91	10.92	7.75	8.16	14.48	1.74	0.98	0.28	0.2610	0.1967	92.90	1.77	0.20	1.33
Fs06-41	MI	90.2	47.51	0.91	10.65	7.67	9.54	13.62	1.90	0.79	0.38	0.2773	0.2205	93.47	2.40	0.28	1.28

Table S1

Auxiliary materials

Table S1. Major and trace element results for standards

	Basalt - BR				Anorthosite - ANG				Serpentine - UBN				Granite - GH				Diorite - DRN			
Element	Number of results	Standard deviation	Working value (%)	95% confidence limits	Number of results	Standard deviation	Working value (%)	95% confidence limits	Number of results	Standard deviation	Working value (%)	95% confidence limits	Number of results	Standard deviation	Working value (%)	95% confidence limits	Number of results	Standard deviation	Working value (%)	95% confidence limits
SiO_2	45	0,98	38,2	0,29	112	0,69	46,3	0,13	48	0,53	39,43	0,15	45	0,61	75,8	0,18	59	0,73	52,85	0,19
Al_2O_3	44	0,4	10,2	0,12	115	0,94	29,8	0,18	50	0,3	2,9	0,08	45	0,35	12,5	0,1	60	0,55	17,52	0,14
Fe_2O_3T	47	0,53	12,88	0,15	127	0,2	3,36	0,04	50	0,36	8,34	0,1	48	0,23	1,34	0,07	64	0,29	9,7	0,07
MnO	42	0,023	0,2	0,007	112	0,01	0,04	0,002	38	0,03	0,12	0,01	41	0,01	0,05	0,002	47	0,02	0,22	0,006
MgO	45	0,42	13,28	0,13	116	0,18	1,8	0,03	48	0,62	35,21	0,18	41	0,1	0,03	0,015	65	0,27	4,4	0,07
CaO	47	0,35	13,8	0,1	119	0,5	15,9	0,09	49	0,11	1,2	0,03	45	0,13	0,69	0,04	70	0,24	7,05	0,06
Na_2O	39	0,25	3,05	0,08	114	0,17	1,63	0,03	30	0,11	0,1	0,04	38	0,22	3,85	0,07	47	0,19	2,99	0,06
K_2O	46	0,14	1,4	0,04	112	0,04	0,13	0,01	36	0,06	0,02	0,01	44	0,15	4,76	0,05	58	0,1	1,7	0,03
TiO_2	43	0,17	2,6	0,05	111	0,04	0,22	0,01	45	0,05	0,11	0,01	42	0,04	0,08	0,01	59	0,08	1,09	0,02
P_2O_5	29	0,06	1,04	0,02	77	0,06	0,01	0,01	26	0,04	0,04	0,02	26	0,01	0,01	0,005	36	0,05	0,25	0,02
H_2O^+	20	0,29	2,3	0,13	35	0,15	0,61	0,05	19	0,47	10,84	0,22	19	0,18	0,46	0,08	17	0,19	2,22	0,09
H_2O^-	20	0,19	0,5	0,08	59	0,05	0,11	0,01	15	0,54	1,26	0,28	18	0,11	0,14	0,05	18	0,1	0,25	0,05
Element	Number of results	Standard deviation	Working value (µg/g)	95% confidence limits	Number of results	Standard deviation	Working value (µg/g)	95% confidence limits	Number of results	Standard deviation	Working value (µg/g)	95% confidence limits	Number of results	Standard deviation	Working value (µg/g)	95% confidence limits	Number of results	Standard deviation	Working value (µg/g)	95% confidence limits
Ba	67	178	1050	44	47	11	34	3,2	31	17,95	27	3	42	32,9	20	3	44	12	385	6
Ce	30	15,5	151	4	32	5,69	4,7	0,4	8	1,84	0,8	0,1	28	16,2	60	3	12	6	46	3
Co	63	11,1	52	3	58	9,14	25	2,4	37	37,19	100	12	24	4,2	0,3	0,1	45	7,8	35	2,3
Cr	82	71,9	380	19	68	10,4	50	3	46	340	2300	100	40	7,4	3	1	48	10,29	40	3
Cs	11	0,5	0,8	0,15	16	0,25	0,05	0,02	14	4,13	10	0,9	19	1	2,5	0,2	14	1,08	6,3	0,6
Cu	68	23,8	72	6	54	4,58	19	1,3	36	8,49	28	3	52	7,2	3	1,5	43	7,18	50	2,2
Dy	9	1,3	6,4	0,2	9	0,34	1,2	0,2	5	0,73	0,38	0,03	11	2,7	12	0,6	6	1,07	4,6	0,4
Er	6	0,5	2,5	0,1	8	0,2	0,75	0,14	5	0,74	0,28	0,02			8	0,4			2,5	0,25
Eu	19	0,7	3,7	0,2	27	0,08	0,37	0,03	11	0,33	0,08	0,01	14	0,1	0,12	0,02	15	0,19	1,45	0,1
Gd	15	1,9	9,5	0,6	9	0,25	0,9	0,17	7	0,99	0,3	0,03	12	2,2	9,5	0,8	13	0,9	4,7	0,5
Hf	9	1,2	5,6	0,2	15	0,05	0,38	0,03					9	1,6	6,6	0,5	7	0,52	3,5	0,3
Ho			1,1	0,13	10	0,11	0,28	0,07			0,09	0,01			2,9	0,3			1	0,1
La	28	17,2	82	1,5	33	0,8	2,2	0,2	9	11	0,35	0,07	25	7,5	25	1	20	3,94	21,5	1,5
Lu	12	0,1	0,25	0,03	22	0,03	0,12	0,01	10	0,18	0,045	0,005	10	0,2	1,1	0,15	12	0,11	0,4	0,06
Nb	20	13,1	98	6	15	1,2	0,7	proposed value	6	0,37	0,05	proposed value	14	9,1	85	5	10	3,08	7	2
Nd	21	15,9	65	2	23	0,28	2,4	0,1	6	0,37	0,6	0,04	18	6,8	29	2	17	2	23,5	1
Ni	84	54,6	260	12	63	9,75	35	3	49	276	2000	80	33	4,8	3	1,5	51	11,05	15	3
Pb	43	7,6	5	2,5	27	3,51	2	1	30	8,59	13	3	44	14,6	45	4,4	30	11,4	55	4
Pr			17	0,6			0,6	0,1			0,12	0,01			7,8	0,5	5	0,49	5,7	0,44
Rb	82	13,7	47	3	38	1,45	1	0,2	19	6,12	4	2	61	33,2	390	10	50	7,62	73	2,2
Sc	18	3,8	25	1,8	27	2,2	10	0,8	12	1,26	13	0,7	19	3,6	9	0,4	15	3	28	1,6
Sm	20	2,8	12,2	0,3	26	0,13	0,7	0,05	7	0,01	0,2	0,01	21	5,2	10	2	16	0,56	5,4	0,28
Sr	94	248,5	1320	51	71	14,84	76	4	31	5,15	9	1,85		0,8	8,7		57	49,6	400	13
Ta	8	1	6,2	0,7	13	0,07	0,18	0,04			0,02	0,005	7	1	4,8	0,4	9	0,17	0,6	0,11
Tb			1,25	0,1	18	0,12	0,2	0,05	5	0,06	0,06	0,01	5	0,3	1,9	0,2	9	0,3	0,77	0,14
Th	20	12,1	11	1	13	0,1	0,04	proposed value			0,07	proposed value	23	19,5	87	8	15	4,56	5	0,4
Tm			0,3	0,04	8	0,08	0,14	0,02			0,045	0,01			1,3	0,1			0,39	0,1
U	14	0,7	2,5	0,3	9	0,75	0,12	proposed value	5	0,49	0,07	proposed value	19	3,4	18	1	13	1	1,5	0,3
V	55	79	235	12	44	13,64	70	4	23	22,2	75	9	20	7,8	5	3	34	34,4	220	11
Y	35	10,5	30	1,5	39	2,34	9	0,75	15	9,07	2,5	0,2	23	37,5	75	3	21	6,96	26	3
Yb	22	1,4	1,8	0,2	28	0,13	0,8	0,05	13	0,54	0,28	0,02	24	2	8	0,6	17	1,33	2,5	0,3
Zn	61	32,6	160	10	55	11,58	20	3	38	21,55	85	7	50	17,4	55	5	47	16,38	145	5
Zr	54	60,3	260	16	46	7,68	11	2,3	14	37,07	4	1	42	65,7	150	20	29	24,83	125	9

Service d'Analyse des Roches et Minéraux, CRPG-CNRS-SARM (France)

Table S2

Auxiliary materials

Table S2. Electron microprobe analyses of S and Cl in reference glasses

	VG2 reference glass				Ke12 pantellerite	
	This work	Reference data			This work	Reference
		[1]	[1]	[2]		[2]
S (ppm)	1479 (31)	1365 (29)	1348 (62)	1450 (30)	na	
n	15	139	134	>50		
Cl (ppm)	300 (3)	316 (19)	291 (52)	300 (35)	3352 (8)	3280 (120)
n	15	139	134	>50	23	

[1] Data compilation from Witter et al., (2005) *Journal of Petrology* 11, 2337-2366, supplementary data

[2] Métrich unpublished data and Spilliaert et al., (2006). Melt inclusion record of the conditions of ascent, degassing and extrusion of volatile-rich alkali basalt during the powerful 2002 flank eruption of Mount Etna (Italy). *Journal of Geophysical Research* 111, B04203.

n: number of analyses

na: not analyzed